scientific reports

Check for updates

OPEN

Simulation of landslide dam failure due to overtopping considering wide-graded soil erosion

Gangyong Song[1]✉, Tianlong Zhao[2,3], Penghui Zhao[4], Changjing Fu[2,5] & Xiong Hu[2]

Landslide dams, as a particular type of secondary geological disaster, can cause serious flood disasters. Therefore, accurately predicting potential dam failure processes is crucial for developing reasonable emergency response plans. Currently, several landslide dam failure models have been proposed, but most of these models do not appropriately consider the wide gradation of landslide dam materials, which is essential for accurate erosion calculations. Therefore, this research proposes a relative exposure formula under three-dimensional conditions to account for the concealment and exposure effects between large and small particles in wide-graded soil. Based on this, the incipient velocity of wide-graded soil is derived, and a mathematical model of overtopping failure of landslide dams is established. As part of the model, a numerical solution process is also developed to ensure convergence. To evaluate the performance of this new mathematical model, the discharge process of Tangjiashan landslide dam was used as a real-world case for dam failure calculation. The calculated results of key dam failure outcomes were compared with actual measurements, showing that the results of this model are largely consistent with actual measurements, with the error controlled within 10%. Additionally, the mathematical model proposed in this article was compared with two other existing dam failure models, revealing that the model proposed here has advantages in controlling the error of key dam failure outcomes, mainly due to the comprehensive consideration of erosion calculation in wide-graded soil. To further evaluate the stability of the model, the breach processes of the "11.3" Baige landslide dam and the Yigong landslide dam were also calculated, and the results showed reasonable consistency. Based on the model presented in this article, the influence of the grading width of landslide dam materials on key dam failure outcomes was discussed. It was found that grading width significantly affects the development process of breach flow. Specifically, wider grading width leads to smaller peak values of breach flow and later peak times. Additionally, the final size of the breach is affected by grading width, as it has a significant impact on erosion strength, although the sensitivity of this parameter is relatively weak. Given the significant impact of grading width on the dam failure process, especially for landslide dams containing wide-graded soil, it is essential to fully consider the wide grading of materials for accurate dam failure calculations.

Keywords Landslide dam, Overtopping failure, Mathematical model, Wide-graded, Soil erosion

Landslide dams are accumulations of soil and rock resulting from geological events like landslides and collapses, obstructing river channels. They possess distinct geometric characteristics, material compositions, and operational conditions compared to artificial soil and rock dams. Geometrically, these accumulations are often irregular, stretching extensively along the river flow direction. Additionally, weak zones within the dam and uneven crests predispose them to initial failure. Structurally, lacking manual consolidation, most dam structures are loose and exhibit pronounced unevenness. The grading range of soil and stone materials within the dam body is wide, with no integrated flood discharge facilities. Consequently, when upstream water inflow elevates the barrier lake's level beyond the dam crest, dam failure becomes imminent[1,2]. Statistical data[3] indicate that the majority of landslide dams eventually breach, with 90% of landslide dams failing within a year. Along the trajectory of this disaster chain, the affected area is likely to continue expanding[4]. Hence, devising a precise

[1]School of Infrastructure Engineering, Nanchang University, Nanchang 330031, People's Republic of China. [2]Key Laboratory for Hydraulic and Waterway Engineering of Ministry of Education, Chongqing Jiaotong University, Chongqing 400074, People's Republic of China. [3]Department of Infrastructure Engineering, University of Melbourne, Parkville, VIC 3010, Australia. [4]Hydrology and Defense Department of Chongqing Water Resources Bureau, Chongqing 401147, People's Republic of China. [5]Department of Civil Engineering, Monash University, Clayton, VIC 3168, Australia. ✉email: gysong_1975@163.com

simulation method to forecast failure progression is crucial for formulating effective emergency response plans for breached landslide dams.

Given the severe flood disasters that can result from dam breaks, the simulation methods for such events have garnered considerable attention from researchers. Mathematical models for earth-rock dam failure can generally be categorized into three types[5,6]:

(1) The first type comprises parametric models based on regression analysis of dam failure case data, and empirical formulas, often employed for quick evaluations of dam failure consequences due to their straightforward formulas and rapid computations[7–12].
(2) The second type encompasses mathematical models based on simplified dam break mechanisms. These models consider the failure mechanisms of earth-rock dams and are widely used in numerical simulations of the failure process[13–18].
(3) The third type involves mathematical models based on refined dam break mechanisms. Some researchers employ sediment transport calculations to simulate the erosion process at the breach[19–23]. This category of model has undergone rapid development in recent years.

While several mathematical models have been proposed for calculating dam failure in earth-rock dams, there remains a scarcity of models specifically tailored for erosion calculations of the wide-graded soil within the landslide dam body. Actually, the development of breaches due to overtopping flow involves sediment transport at a meso-scale level. Existing sediment transport models used in mathematical models for dam breaches predominantly describe this physical process using current sediment transport formulas. However, these models are typically developed based on studies of sediment transport in riverbeds, where the particle sizes are relatively uniform. This grading significantly differs from the natural soil and rock masses found in landslide dams. Therefore, directly applying existing sediment transport equations for calculating sediment transport during dam breaches has considerable limitations. Additionally, prior studies[24] have highlighted the significant impact of soil and sand gradation characteristics on their initiation and transport. Hence, it is pertinent to undertake erosion calculation research focusing on the unique grading of landslide dam materials and establish a model for landslide dam failure.

This study aims to present a novel mathematical model for simulating the failure of landslide dams caused by overtopping, integrating an erosion equation of wide-graded soil (Sect. 2). As part of the breach model, a numerical scheme is developed to ensure the convergence of model calculations (Sect. 3). The model's performance is evaluated through a real-world case study and compared with two existing models (Sect. 4). Furthermore, the assumptions and limitations of this study are discussed (Sect. 5), and based on the findings, recommendations for future research are provided (Sect. 6).

Model development

Breach erosion considering wide-graded soil transport

Researchers commonly introduce particle exposure to calculate the incipient velocity of non-uniform sediment[25]. However, when discussing the exposure of non-uniform sand, there is no fixed reference plane, and most researchers employ the horizontal plane as the reference for exploration. However, this assumption is too simplistic for capturing the movement of soil particles in landslide dam failures, especially in scenarios with steep riverbed slopes or significant disparities in particle sizes.

In this study, it is assumed that the reference plane for particle exposure is the average bed plane of the riverbed, and exposure is defined as the degree of particle exposure relative to that bed plane. The average bed plane slope of the riverbed varies with different slopes, as illustrated in (Fig. 1a). In Fig. 1b O_1, O_2, O_3 and O_4 represent the center of gravity of soil particles, while C, D, and E denote the contact points between the studied particle O_1 and the lower layer particles O_2, O_3, and O_4. Point B marks the intersection point AB of the vertical plane where the center of gravity of soil particles O_1 is located and the riverbed plane. Line segment O_1B is perpendicular to AB.

Furthermore, in Fig. 1c, D and E represent the contact points between particle O_1 and downstream particles O_2 and O_3, respectively. The angle α, between the line segment O_1A perpendicular to the center of gravity of

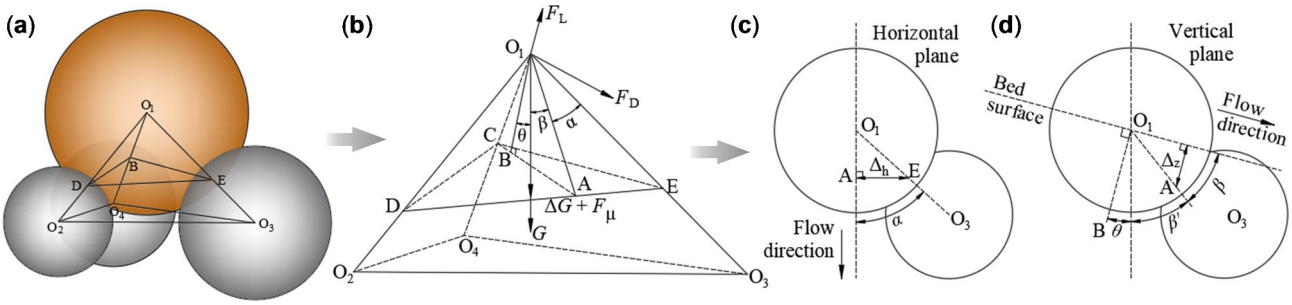

Fig. 1. Particle exposure analysis: (**a**) Spatial position of soil particles; (**b**) Force analysis on particle O_1; (**c**) The planar positional relationship of soil particles; (**d**) The vertical position relationship of soil particles.

particle O_1 and the line connecting particles O_1 and O_3, is referred to as the lateral exposure angle of soil and gravel, with a range of values from 0 to 90°.

Additionally, in Fig. 1d, β denotes the angle between O_1A and the vertical direction, where $\beta+\theta$ represents the residual angle of the longitudinal exposure angle. Thus, the longitudinal exposure angle β satisfies the equation $\beta=90\text{-}\beta'\text{-}\theta$, with a range of values from 0 to 90°.

When $\beta=90°$, the sediment particles are completely exposed, while sediment particles are in a completely concealed state when $\beta=0°$.

If the horizontal exposure is defined as $\Delta_h=\frac{1}{2}D\sin\alpha$ and the vertical exposure is defined as $\Delta_z=\frac{1}{2}D\sin\beta$, then the absolute exposure of particles is:

$$\Delta=\frac{D}{2}\sqrt{(\sin\alpha)^2+(\sin\beta)^2} \tag{1}$$

where D represents the diameter of particle O_1. Since the horizontal and vertical distributions of particles in the landslide dam are similar[26], for simplification purposes, it is assumed that $\alpha=\beta$. In this case, Eq. (1) can be written as:

$$\Delta=\frac{\sqrt{2}}{2}D\sin\alpha \tag{2}$$

It is evident from the formula above that besides the transverse and longitudinal exposure angles, particle size significantly influences the absolute exposure of particles. In this study, we defines the relative exposure as $\Delta\prime=\frac{2\Delta}{D}$, thus the expression for the relative exposure of particles is:

$$\Delta\prime=\sqrt{2}\sin\alpha \tag{3}$$

In Fig. 1b, the forces acting on soil particle O_1 include: drag force (F_D), uplift force (F_L), gravity (G), adhesion force (F_μ), and additional downward force (ΔG). The direction of F_D aligns with the direction of water flow, F_L is perpendicular to the water flow direction, while F_μ, ΔG, and G act vertically downward. The expressions for each physical quantity are as follows:

$$\begin{cases} F_D=C_DA_DD^2\dfrac{\rho\left(v_c-v_x\right)^2}{2} \\ F_L=C_LA_LD^2\dfrac{\rho\left(v_c-v_x\right)^2}{2} \\ G=\left(\gamma_s-\gamma_w\right)\dfrac{\pi D^3}{6} \\ \Delta G=\dfrac{\sqrt{3}}{2}\pi K_2\gamma_wHD\left(3-\dfrac{s}{\delta_1}\right)\left(\delta_1-s\right) \\ F_\mu=\dfrac{\sqrt{3}}{4}\pi cD\delta_0^3\left(3-\dfrac{s}{\delta_1}\right)\left(\dfrac{1}{s^2}-\dfrac{s}{\delta_1^2}\right) \end{cases} \tag{4}$$

In Eq. (4), v_c denotes the instantaneous velocity of water flow; v_x signifies the velocity of sediment particles; C_D stands for the drag force coefficient of water flow, considered as 0.4[27], A_D represents the drag force area effect coefficient, with $A_D=\pi/4$; C_L denotes the lifting force coefficient of water flow, set as 0.1[27], A_L signifies the coefficient of action of the lifting force area, taken as $\pi/4$; ρ represents the density of water; γ_s represents the bulk density of soil materials; γ_w signifies the bulk density of water; H indicates the elevation of the reservoir water level before the dam; K_2 is set to 2.258×10^{-3}, according to Li (2018)[28]; δ_1 represents the thickness of the thin film water, valued at 4×10^{-7} m (Li et al., 2018); δ_0 represents the thickness of a water molecule, with a value of 3×10^{-10} m (Li et al., 2018); s signifies the gap between soil particles, with a value of $0.25\delta_1$[27]. c represents cohesion. The force arms for each force are as follows:

$$\begin{cases} L_D=\Delta+\dfrac{D}{6}=\dfrac{D}{6}\left(3\Delta\prime+1\right) \\ L_L=\dfrac{D}{2}\cos^2\alpha \\ L_G=\dfrac{D}{2}\cos\alpha\cos\left(\alpha+\theta\right) \end{cases} \tag{5}$$

Assuming that the additional downward pressure (ΔG) and adhesion force (F_μ) of soil particles with larger size are zero, and the sediment movement velocity before initiation $v_x=0$. At the critical state, according to the torque balance equation $F_DL_D+F_LL_L=\left(G+\Delta G+F_\mu\right)L_G$, the critical water flow velocity for soil particle initiation is obtained as:

$$v_c=\sqrt{\frac{4D\left(\gamma_s-\gamma_w\right)+24\left(\Delta G+F_\mu\right)}{\left[C_D\rho\left(3\Delta\prime+1\right)+3C_L\rho\left(1-\frac{\Delta\prime^2}{2}\right)\right]\Big/\left[\left(1-\frac{\Delta\prime^2}{2}\right)\left(\cot\theta-\frac{\Delta\prime}{\sqrt{2-\Delta\prime^2}}\right)\sin\theta\right]}} \tag{6}$$

When $D > 0.5$ mm, the thin films of water surrounding each soil and gravel particle do not come into contact with each other. At this point, $F_{il} = 0$ and $\Delta G = 0$ (Li et al., 2018). For the relative exposure of wide-graded soil and rock particles inside the landslide dam, the analysis can be conducted using a relative exposure distribution function[27]. By integrating the distribution function, the expected relative exposure of particles for each particle group can be obtained as follows:

$$\overline{\Delta\prime}_l = \begin{cases} 1 - \frac{1}{2}\left(\frac{\frac{\overline{D}}{D_l} - \Delta\prime_m^2}{\frac{\overline{D}}{D_l} - \Delta\prime_m}\right), & D_l \le \overline{D} \\ 1 - \frac{1}{2}\left(\frac{\overline{D}}{D_l} + \Delta\prime_m\right), & D_l > \overline{D} \end{cases} \tag{7}$$

In the equation, $\overline{D}$ represents the average particle diameter, denoted by d_{50}, D_l denotes the average particle diameter of the particle group l, $\Delta\prime_m$ represents the minimum value of the relative exposure of particles, and the value is 0.134 when densely packed. The comprehensive relative exposure of particles can be determined through a weighted averaging method:

$$\overline{\Delta\prime} = \sum_{l=1}^{n_p} \overline{\Delta\prime}_l P(\Delta\prime_l) \tag{8}$$

where, n_p represents the number of particle groups, and $P(\Delta\prime_l)$ represents the content of particles in the particle group l. In response to the breaching water flow, erosion will manifest at the top breach and downstream slope of the barrier dam. Considering the wide gradation of the landslide dam material, we propose an empirical expression to compute the erosion rate (Q_s):

$$Q_s = 0.25\left(\frac{d_{90}}{d_{30}}\right)^{0.2} B \sec\theta \frac{v_* \left(v_b^2 - v_c^2\right)}{g\left(\frac{\gamma_s}{\gamma_w} - 1\right)} \tag{9}$$

In which,

$$\begin{cases} v_b = \overline{v}\left(\frac{d_{90}}{H - H_c}\right)^{\frac{1}{6}} \\ v_* = \overline{v} N \sqrt{g(H - H_c)^{-\frac{1}{3}}} \\ \overline{v} = \frac{Q_b}{B(H - H_c)} \end{cases} \tag{10}$$

Here, d_{90} and d_{30} represent different particle sizes, indicating that the mass of particles smaller than d_{90} or d_{30} accounts for 90% or 30% of the total weight, respectively. B stands for the width of the breach, v_b, v_*, $\overline{v}$ denote the bottom flow velocity, frictional flow velocity, and average flow velocity at the breach, respectively. H_c indicate the elevation of the bottom of the breach. N represents the roughness coefficient at the breach.

Breach discharge and expansion

Assuming the initial breach cross-section is trapezoidal, based on previous research findings[14,15,29,30], the longitudinal and transverse development pattern of the breach is depicted in Fig. 2. Therefore, within the time increment Δt_i, the incremental depth of the breach's bottom cut can be derived as follows:

$$\Delta H_{ci} = \frac{\Delta t_i Q_s}{\overline{B_i} L (1 - n)} \tag{11}$$

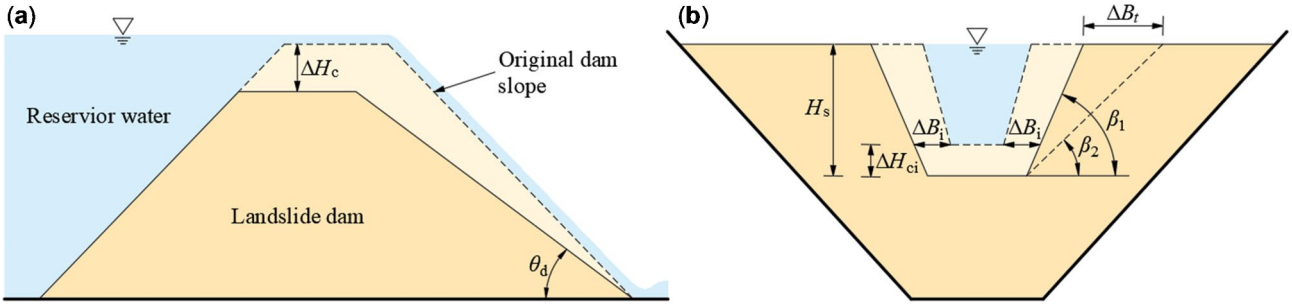

Fig. 2. Illustration of the landslide dam failure process caused by overtopping: (**a**) Cross-sectional diagram; (**b**) The downstream elevation view.

where $\overline{B_i}$ is the average bottom width of the breach; L represents the sum of the top width of the dam and the downstream slope length; and n denotes the porosity of the dam material. The depth of undercut of the breach is given by:

$$\Delta H_c = \sum_{i=1}^{n_T} \Delta H_{ci} \tag{12}$$

where n_T represents the total number of iterations.

If we neglect the lateral expansion of the breach induced by the instability and collapse of the breach slope, the erosion rate at the bottom of the breach should be approximately equal to that of the breach slope. Therefore, it is assumed that the depth and width of the breach develop at the same rate. Consequently, the increment of the breach width, ΔB, formed by the direct erosion of the water flow on both sides of the dam breach, as depicted in Fig. 2b, can be expressed as:

$$\Delta B = \sum_{i=1}^{n_T} 2\Delta B_i = 2\Delta H_c \tag{13}$$

The breach is continuously undergoing vertical undercutting and lateral expansion under the continuous erosion of the diffuse dam current, and the side walls on both sides of the breach become steeper and steeper. Once the vertical undercutting reaches the critical angle, the side walls on both sides of the breach will intermittently collapse, as depicted in (Fig. 2b). The critical angle can be determined using the limit equilibrium method of soil stability. Assuming that the instability and collapse of the breach slope result in planar sliding, the downward force and resisting force of the potential sliding mass, according to the geometric relationship depicted in Fig. 2b, can be expressed as:

$$\begin{cases} F_d = W \sin\beta_1 = \dfrac{1}{2}\gamma_s H_s^2 \left(\dfrac{1}{\tan\beta_2} - \dfrac{1}{\tan\beta_1}\right) \sin\beta_2 \\ F_r = W \cos\beta_2 \tan\varphi + \dfrac{cH_s}{\sin\beta_2} = \dfrac{1}{2}\gamma_s H_s^2 \left(\dfrac{1}{\tan\beta_2} - \dfrac{1}{\tan\beta_1}\right) \cos\beta_2 \tan\varphi + \dfrac{cH_s}{\sin\beta_2} \end{cases} \tag{14}$$

In Eq. (14), F_d represents the downward force, F_r represents the resisting force (considering both frictional and cohesive components), W is the gravity of the sliding soil mass, H_s is the depth of the breach, c is the cohesive strength of the dam material, φ is the internal friction angle of the dam material, β_1 is the critical slope angle of breach instability, and β_2 is the new slope angle formed after the instability and collapse of the breach slope. At the critical equilibrium state, $F_d = F_r$. Substituting this into Eq. (14) yields the critical slope angle of breach instability as follows:

$$\tan\beta_1 = \frac{\frac{1}{2}\gamma_s H_s^2 \cos\beta_2 \tan\varphi - \frac{1}{2}\gamma_s H_s^2 \sin\beta_2}{\frac{\gamma_s H_s^2 \cos\beta_2 \tan\varphi}{2\tan\beta_2} - \frac{1}{2}\gamma_s H_s^2 \cos\beta_2 + \frac{cH_s}{\sin\beta_2}} \tag{15}$$

At this point, the increment of breach width expansion caused by the intermittent instability and collapse of the breach slope can be calculated using the following equation:

$$\Delta B_t = H_s \left(\frac{1}{\tan\beta_2} - \frac{1}{\tan\beta_1}\right) \tag{16}$$

The model employs the broad-top weir equation to compute the discharge of breach as:

$$Q_b = k_s \left[c_1 B (H - H_c)^{1.5} + c_2 m (H - H_c)^{2.5}\right] \tag{17}$$

In the equation, k_s is the submergence coefficient, c_1 and c_2 are correction factors, with values taken from Singh (1984)[31] as 1.7 and 1.3 respectively, and m represents the slope coefficient of the breach. H_c denotes the elevation of the bottom of the breach. Then, the flow velocity v_b of the breach water can be expressed as:

$$v_b = \frac{Q_b}{S_a} \tag{18}$$

where S_a represents the cross-sectional area of the breach. The change of reservoir water level during time period Δt_i is:

$$\Delta H = \sum_{i=1}^{n_T} \frac{(Q_{in} - Q_b)\,\Delta t_i}{S_r} \tag{19}$$

where S_r represents the area of the reservoir surface corresponding to the reservoir water level of H, and Q_{in} denotes the inlet flow to the reservoir.

Numerical scheme

The model employs an iterative method based on time steps for execution. By inputting initial conditions, boundary conditions, and parameters of the landslide dam and lake, the model calculates the progression of dam break due to overtopping. The calculation process unfolds as follows:

(1) Inputting Initial Conditions, Boundary Conditions, and Calculation Parameters. This includes dam dimensions (height, top width, upstream and downstream slope ratios), breach parameters (initial width, initial depth), dam material properties (particle size, specific gravity, porosity, clay content, cohesive strength), fluid parameters (fluid density, dynamic viscosity coefficient), reservoir capacity information, downstream channel information (water level).
(2) Set Δt.
(3) Make $t = t + \Delta t$.
(4) Calculate the critical sediment transport velocity v_c using Eq. (6), and compute the flow velocity v_b of the breach water using Eq. (18).
(5) Check if $v_b > v_c$. If not, output the final breach bottom elevation H_{cf}, final breach width B_f, final reservoir water depth H_f and breach discharge Q_b. If yes, proceed to the next step.
(6) Calculate the erosion rate Q_s at the breach using Eq. (9). Compute the incremental breach depth ΔH_c and breach width ΔB using Eqs. (12) and (13) respectively.
(7) Verify if the breach slope angle $\beta_b < \beta_1$. If not, set $\beta_b = \beta_2$ and return to step (3). If yes, proceed to the next step.
(8) Check if the elevation of the breach bottom $H_c \leq H$. If not, return to step (3). If yes, proceed to the next step.
(9) Output the final breach bottom elevation H_{cf}, final breach width B_f, final reservoir water depth H_f and breach discharge Q_b.

The iterative calculation process of the model is shown in Fig. 3.

Case studies

Validation of the sediment transport equation

From a meso-scale perspective, the breach process of an embankment dam can essentially be attributed to the complex phenomenon of sediment transport, in which the breach flow carries dam materials downstream. Given this, the accuracy of the sediment transport equation (Eq. 9), which describes this physical process, is crucial for ensuring the precision of breach calculations. The sediment transport equation is derived based on the sediment incipient motion velocity equation (Eq. 6). Therefore, it is essential to first validate the incipient motion velocity of the sediment.

In traditional studies on sediment transport, the calculation and measurement of incipient motion velocity differ from those in dam breach studies, as the former typically use the depth-averaged velocity rather than the instantaneous velocity. Dou[32] proposed that there is a relationship between the instantaneous velocity v_c and the time-averaged velocity $\overline{v}_c$, as follows:

$$v_c = (1 + 0.37n)\,\overline{v}_c = \lambda \overline{v}_c \tag{20}$$

Dou[32] defined the incipient motion states of soil and rock materials based on different values of n, where $n = 1$, 2, 3 correspond to weak, moderate, and general motion of the bed materials, respectively. When the incipient motion state is weak, λ=1.37,for moderate motion, λ=1.74; and for general motion, λ=2.11. Bai's[33] research indicates that the time-averaged velocity near the bed in an open channel satisfies the following relationship with the friction velocity:

$$\begin{cases} \overline{v}_c = \varphi v_* \\ \varphi = 5.75\lg\left(30.2\dfrac{y\chi}{K_s}\right) \end{cases} \tag{21}$$

In which, y=2D/3, χ=1, K_s=2D。 Han[34] proposed that the depth-averaged velocity U and the friction velocity v_* follow the exponential relationship shown below, which can be expressed as:

$$\frac{U}{v_*} = \frac{U}{\sqrt{gHJ}} = 6.5\left(\frac{H}{D}\right)^{\frac{1}{4+\lg\left(\frac{H}{D}\right)}} \tag{22}$$

Substituting Eqs. (20) and (21) into Eq. (22) yields the following:

$$U = \frac{6.5 v_c}{\varphi\lambda}\left(\frac{H}{D}\right)^{\frac{1}{4+\lg\left(\frac{H}{D}\right)}} \tag{23}$$

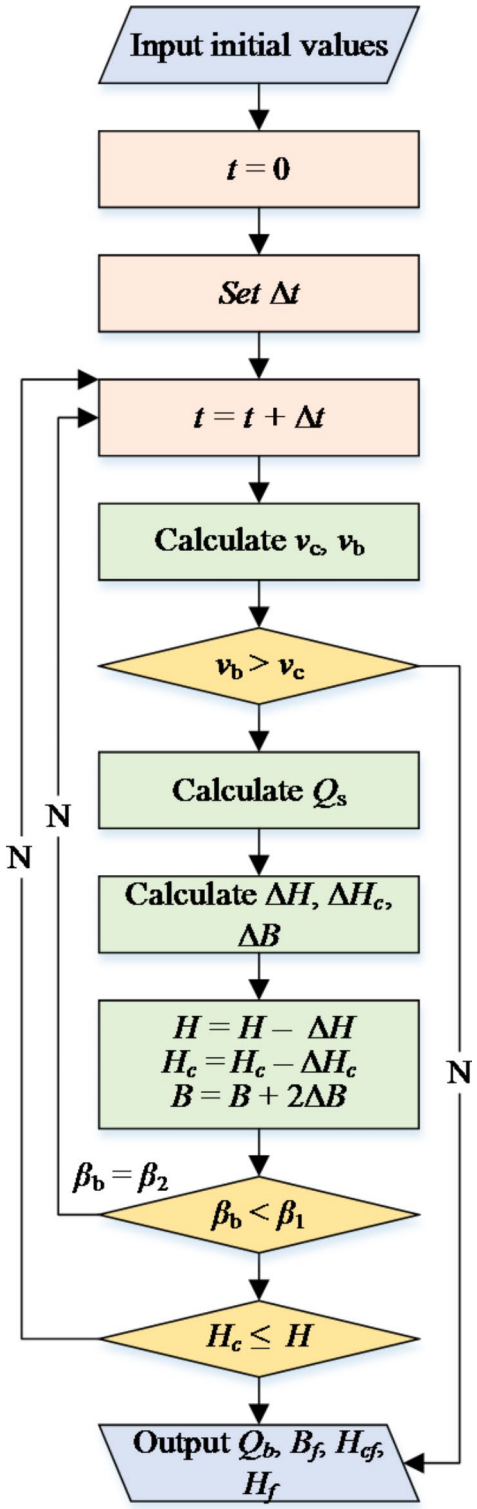

Fig. 3. Flowchart of the numerical calculation process in the model.

In which, v_c can be calculated using Eq. (6) from this study. This study selected both uniform and non-uniform sands to validate the incipient motion velocity formula proposed in this paper. For uniform sand, the validation was conducted using Tang's formula (1963) for sediment particles, along with measured velocities obtained by researchers. For non-uniform sand, Han's formula[34] and field data from hydrological stations were employed for validation. The existing incipient motion velocity expressions used in this validation are presented in Table 1.

The density of sediment particles is 2650 kg/m^3, and the water depth is 0.15 m. For uniform sand, the bed slope θ=0°, the exposure degree of sediment particles is α=0°, β=0°, and λ=1.74, with a particle size range of

Sand type	Proposer	Expression	Remarks
Uniform sand	Cunben Tang[52]	$U=\frac{(\gamma_s-\gamma)gD}{\gamma}\left(6.25+41.6\frac{h}{h_a}\right)+\left(111+740\frac{h}{h_a}\right)\frac{h_a\delta g}{D}$	h_a represents atmospheric pressure expressed in terms of a water column, with a value of 10; δ represents the thickness of a water molecule, with a value of 3×10^{-1} m
Non-uniform sand	Qiwei Han[34]	$U=0.0802f(\lambda)\varphi(\Delta I)\phi\left(\frac{H}{D}\right)\omega_0$	

Table 1. The existing critical flow velocity expression used for validation.

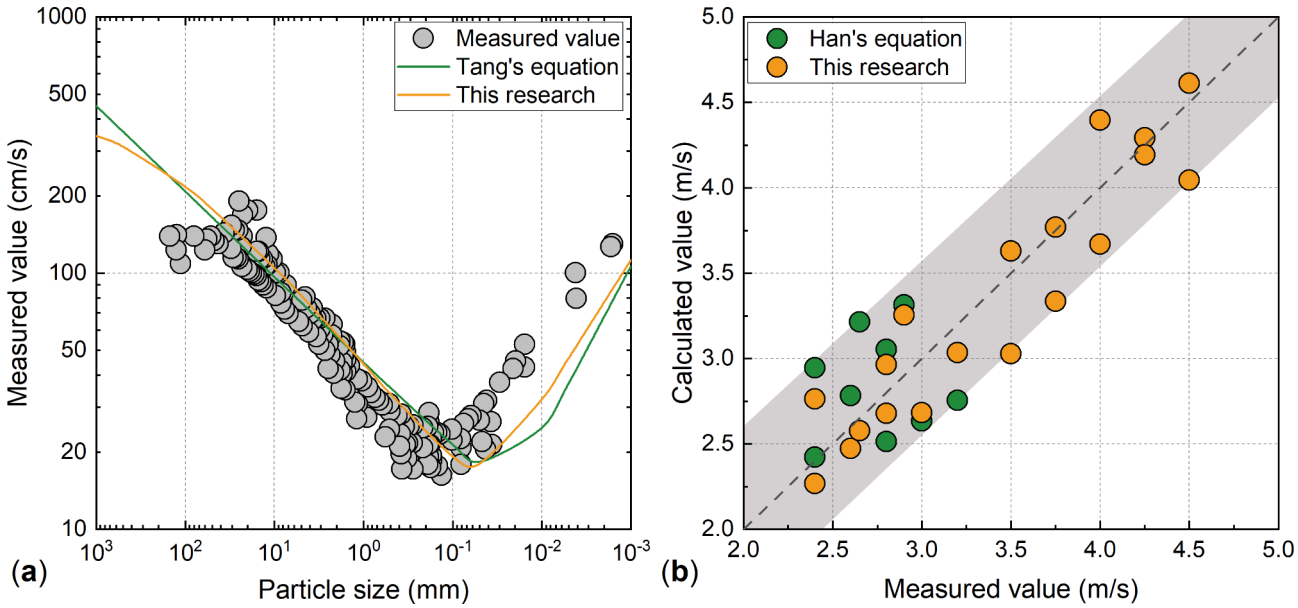

Fig. 4. Validation of the vertical-averaged critical flow velocity formula: (**a**) uniform sand; (**b**) non-uniform sand.

0.001-1000 mm. For non-uniform sand, calculations and validations were conducted based on the field data of incipient motion velocities for non-uniform sand from the Changjiang (Yangtze River) Cuntan Hydrological Station, Wanzhou Hydrological Station, and Yichang Hydrological Station mentioned in reference[27]. The calculation results are presented in Fig. 4.

From Fig. 4a, the calculated incipient motion velocities for uniform sand using the formulas proposed in this paper closely match the measured results. However, it should be noted that these calculations do not consider the effect of particle exposure on incipient motion velocity. Furthermore, under the condition of a water depth of 0.15 m, the critical particle size for incipient motion velocity is approximately 0.1 mm. This implies that when the particle size exceeds 0.1 mm, the critical incipient motion velocity increases with larger particle sizes. Conversely, when the particle size is less than 0.1 mm, the incipient motion velocity exhibits the opposite trend; that is, as the particle size decreases, the critical incipient motion velocity gradually increases. As shown in Fig. 4a, the calculated critical particle size in this study is slightly smaller than the measured data (0.17 mm). When the particle size is below this critical size, the calculated incipient motion velocity is slightly lower than the measured values. This discrepancy can be attributed to the fact that the gap between soil particles, $s=0.25\delta_1$, may need adjustment when applied to clay, as the current value clearly underestimates the resistance due to intermolecular forces during the initiation process, resulting from an excessively large particle gap value. However, for landslide dams, determining the appropriate value for the gap between soil particles remains a significant challenge. According to Fig. 4b, when calculating the incipient motion velocity for non-uniform sand using the formulas developed in this study, the results are relatively close to the measured values. This agreement can primarily be attributed to the consideration of the blocking and shielding effects of larger particles on smaller particles, as well as the encasing and filling effects of smaller particles on larger particles. Consequently, the calculated incipient motion velocity results align more closely with the measured data.

The calculation of sediment transport rates is directly related to the rate of breach expansion, which in turn affects the development process of breach flow. Therefore, it is essential to validate the sediment transport rate formula proposed in this study (Eq. 9). By selecting specific parameter values detailed in Appendix A–D, the reliability of the formula was confirmed through experimental data obtained from flume tests[35].

As shown in Fig. 5, the calculated unit width sediment transport rates for four different soil types generally fall within the range of observed test values. Thus, the proposed formula can accurately estimate sediment transport caused by overtopping failure in landslide dams. It is noteworthy that, compared to the slightly underestimated values in Figs. 5a and b), the consistency between the calculated and measured results in Figs. 5c and d is significantly better. This can be primarily attributed to the fact that the erosion formula proposed in this study was specifically developed for coarse-grained sediment conditions, making it more suitable for coarse-grained sediments rather than fine-grained sediments. However, for fine-grained sediments, the mode's calculated values still fall within the range of experimental variability. Therefore, the sediment transport formula proposed in this study is also considered to be effective.

Tangjiashan landslide dam

The data obtained during the mitigation process of the Tangjiashan landslide dam, formed by the 2008 Wenchuan earthquake in Sichuan, were utilized to validate the mathematical model and calculation method proposed in this study. Following the Wenchuan earthquake, a trapezoidal drainage channel was excavated at the crest of the Tangjiashan landslide dam by June 1, 2008, through manual excavation to alleviate the risk. The slope of both sides of the channel is 1:1.5, the elevation of the bottom is 740.0 m, the bottom width is 8 m, the depth is 13 m, the total length is 695 m, and the material consists mainly of layered fragmented rock (as illustrated in Fig. 6).

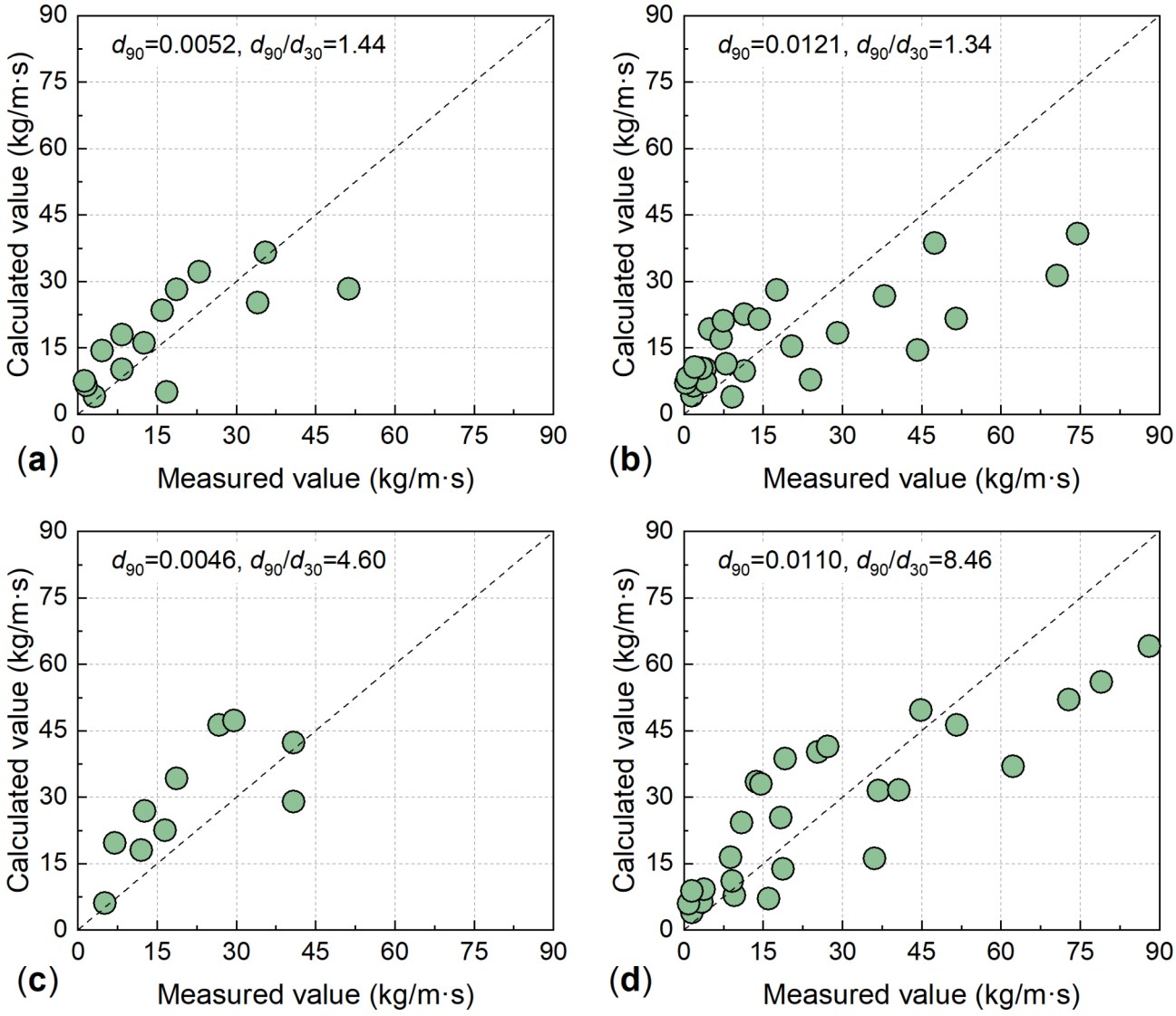

Fig. 5. Validation of the sediment transport rate formula: (**a**) $d_{90}/d_{30}=1.44$; (**b**) $d_{90}/d_{30}=1.34$; (**c**) $d_{90}/d_{30}=4.6$; (**d**) $d_{90}/d_{30}=8.46$.

Based on the remote sensing monitoring images combined with DEM calculations[36,37]), the relationship curves of water level, backwater area, and reservoir capacity in front of Tangjiashan landslide dam were obtained, as depicted in Fig. 7.

According to data provided by Liu[38] and Hu[39], the material comprising the Tangjiashan landslide dam is primarily gravel. In fact, when the dam was formed, large boulders with diameters of several meters were scattered on the surface. During the excavation of the spillway, to expedite the process and mitigate risks as quickly as possible, a combination of blasting and excavation methods was employed[40]. In this process, some of the large boulders were fragmented by blasting. Additionally, most of the large boulders were located on the surface of the dam, while the breach erosion mainly occurs from the bottom of the breach and scours downward. Therefore, the influence of these large boulders was not considered in the breach process calculations. In this study, soil grading tests of the matrix of the landslide debris were conducted by the Chengdu Hydropower Design Institute, China Hydropower Consulting Group Corporation, using samples taken from pits and boreholes[38], and the results are shown in Table 2. Chen[14] also performed calculations on the draining process of the Tangjiashan landslide dam, using grading curves that fell within the upper and lower bounds of Liu's[38] results. Thus, this study adopted the material grading curve from Liu's research for parameter calculations of the dam material.

According to Table 2, the average particle diameter of the Tangjiashan landslide dam is $\overline{D} = 23.11$ mm. The average particle diameter D_l of each particle group is calculated as the average of the boundary particle diameters of adjacent groups. The content and average relative exposure of each particle group are also listed in Table 2. The other specific foundational parameters of the landslide dam are presented in Table 3. It is important to note that different researchers have provided varying descriptions of the parameters for the Tangjiashan landslide dam. For instance, Liu[38] reported that the dam height, measured at the highest crest surface of the left deposit, was 124.3 m, while at the lowest crest surface of the right deposit, it was 90.0 m. Chang[13] described the dam height as ranging from 82 to 124 m, and Zhong[41], in their calculations, adopted a value of 103 m. To ensure comparability between our results and those of Zhong and Chang, we have chosen the dam height based on Zhong's[41] value.

The iterative calculation method is employed to numerically calculate the discharge process (as illustrated in Fig. 3), with a selected iterative calculation time step of $\Delta t = 1$ s. The calculation commences from the erosion of soil and rock particles in the discharge channel at 6:00 on June 10, 2008, and the calculation duration is set to 36.1 h. The calculation outcomes are depicted in Fig. 8.

Figure 8 illustrates the comparison between the calculated and measured drainage processes. Regarding the breach discharge, during the initial phase, the calculated breach discharge rate increases slowly, resulting in a final total discharge volume smaller than the actual total discharge volume. Based on the data, the calculated peak flow rate is 6698 m^3/s, occurring 14.17 h after discharge, with a discharged volume of 1.65×10^8 m^3; while the measured peak flow rate is 6505 m^3/s, occurring 15.16 h after discharge, with a discharged volume of 1.85×10^8 m^3. Regarding the development of the breach, after the dam release, the cross-section of the breach appears trapezoidal. The calculated final breach widths are all within the measured range, although the calculated values tend to be closer to the lower limit of the range. According to the data, the measured final breach top width ranges from 145 to 225 m, and the bottom width ranges from 100 to 145 m. The calculated breach development process is depicted in Fig. 8c, with a final top width of 149.24 m and bottom width of 103.90 m. Overall, the calculated results are largely consistent with the measured values, indicating that the model proposed in this study is applicable for landslide dam breach and discharge calculations.

To further evaluate the performance of the model proposed in this study in real-world case applications, we selected the discharge of the Tangjiashan landslide dam as a case study and compared the calculation results

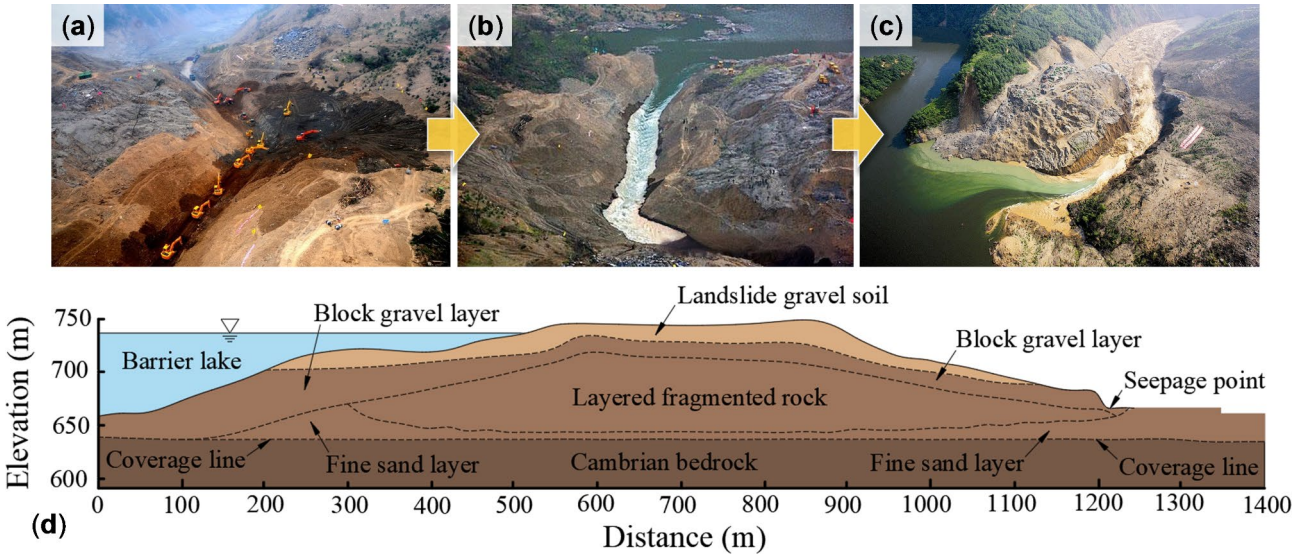

Fig. 6. Tangjiashan landslide dam: (**a**) Excavation of discharge channel; (**b**) Initial discharge; (**c**) Dam breaching (Courtesy of Guoying Li); (**d**) Engineering geological longitudinal profile[14,15].

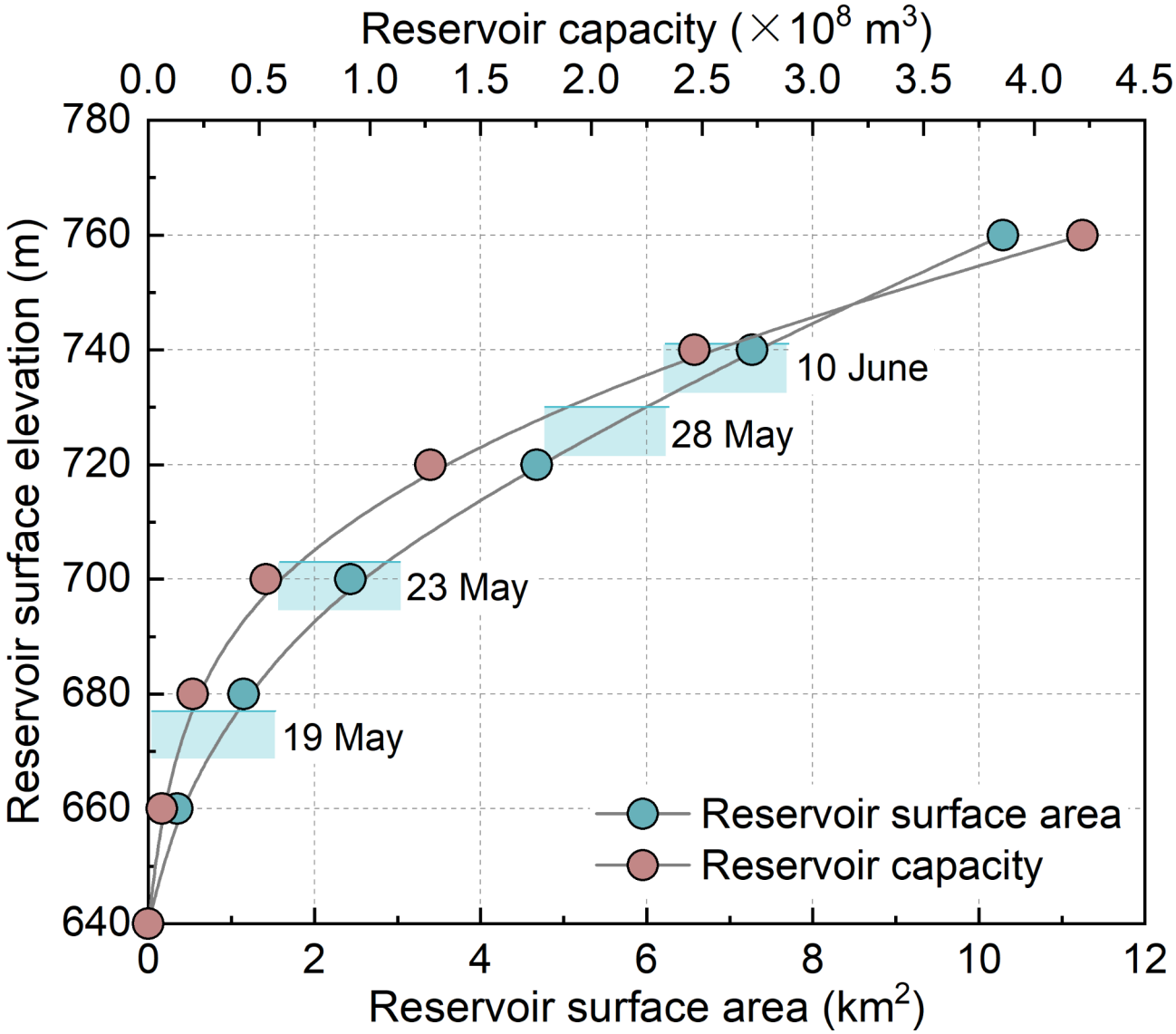

Fig. 7. The Tangjiashan lake water level-surface area-storage capacity relationship.

Particle size (mm)	The content of particle groups (%)						$\overline{\Delta}_l$
	Borehole 1#	Borehole 2#	Borehole 3#	Borehole 4#	Borehole 5#	$P(\Delta'_l)$	
0.005	5.27	3.77	7.08	5.87	1.36	4.67	0.49999
0.075	9.49	6.93	12.80	9.19	2.11	8.10	0.49990
0.25	2.86	5.12	6.17	4.97	2.86	4.40	0.49959
0.5	1.36	1.96	2.11	1.20	0.75	1.48	0.49906
2	3.61	8.13	7.08	6.33	2.26	5.48	0.49684
5	6.48	12.50	12.80	10.99	3.92	9.34	0.49103
10	6.17	11.45	4.07	7.23	5.57	6.90	0.48031
20	8.58	9.94	5.87	8.28	9.94	8.52	0.45875
40	8.13	8.13	4.97	6.48	7.98	7.14	0.54783
60	5.72	2.56	3.92	4.22	2.11	3.70	0.70190
100	16.87	21.08	33.13	26.51	24.40	24.40	0.78856
200	25.45	8.43	0.00	8.73	17.32	11.99	0.85597
250	0.00	0.00	0.00	0.00	19.43	3.89	0.88164

Table 2. The particle composition of the Tangjiashan landslide dam.

Parameters	Values	Parameters	Values
Dam height (m)	103	γ_w (kN/m^3)	9.8
Crest width (m)	300	γ_s (kN/m^3)	26
Dam length (m)	612	c (kPa)	25[a]
U/S slope (V/H)	0.36	φ (°)	22
D/S slope (V/H)	0.24	n	40%
Reservoir storage (m^3)	1.5×10^8	C_L	0.1
Initial reservoir lever (m)	92.5	C_D	0.4
Initial downstream water lever (m)	0[a]	A_D	π/4
Initial breach depth (m)	13	D_L	π/4
Initial breach width (m)	8	θ (°)	13.5

Table 3. Conditions of Tangjiashan landslide dam. [a]Assumed values.

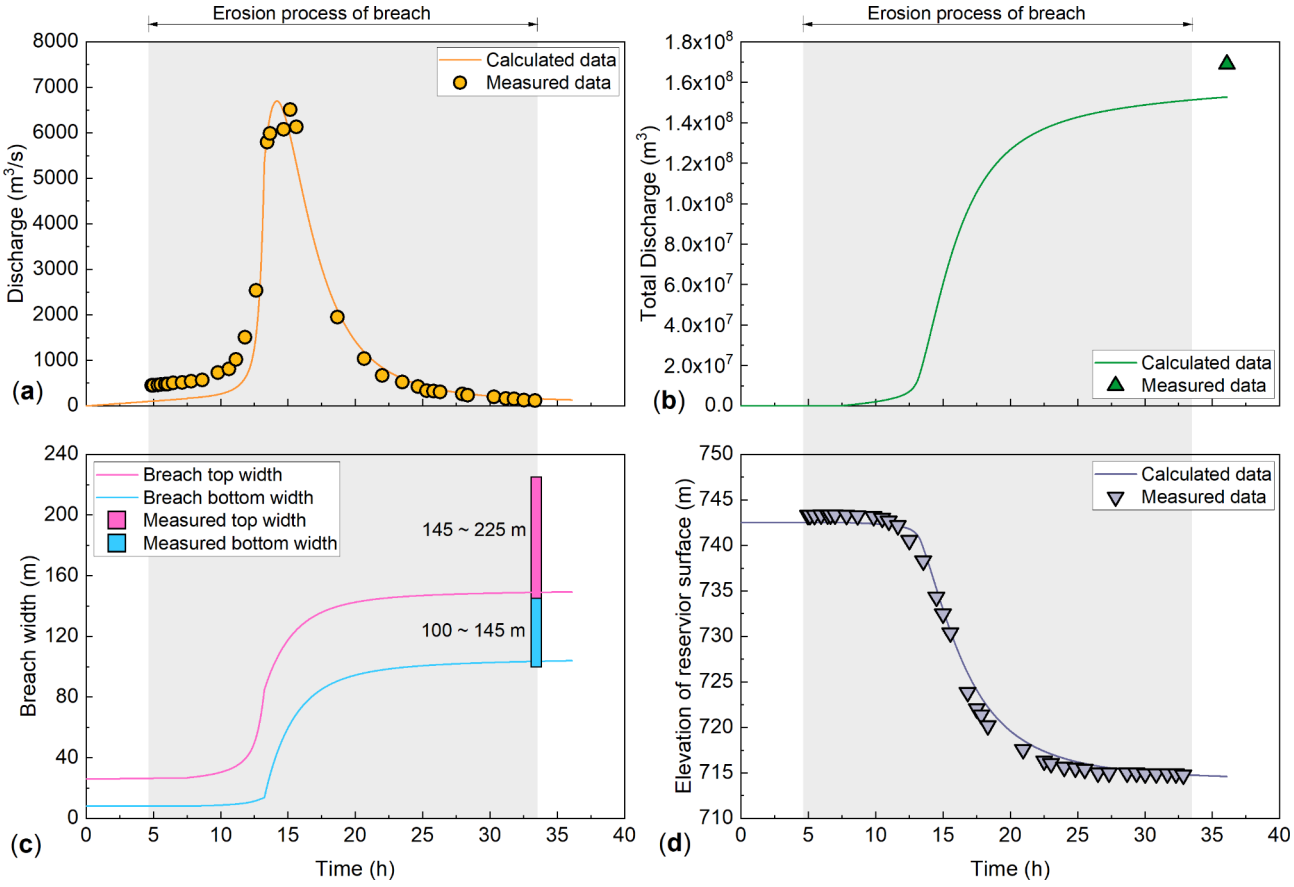

Fig. 8. Calculation results of Tangjiashan landslide dam discharge process: (**a**) Discharge of breach; (**b**) Development of total discharge volume; (**c**) Development of breach; (**d**) Development of reservoir water level.

of this article with those of two existing breach models[13,41]). The comparative parameters mainly include key outcomes of the dam failure process, such as peak flow Q_p, peak occurrence time T_p, final breach top width B_t, final bottom width B, and final depth H_s. In Zhong's model, the final depth of the breach was not output as a result but was used as an input parameter in the calculation, so this value is not listed here. Chang's model does not provide the peak time, so no comparison is made here. The comparison results are shown in Table 4.

According to the comparison results, all three models can depict the overtopping failure of landslide dams. Compared with the other two dam failure models, model proposed in this research considers the impact of erosion by wide-graded particles on the dam failure process, especially the influence of shielding and exposure between particles with different sizes on the initiation flow velocity. This ensures that the key results of dam failure calculations are controlled within a 10% error range, indicating relatively high accuracy. Moreover, this model further improves calculation precision based on previous studies. The improvement in calculation precision is primarily attributed to the model's thorough consideration of the interactions between coarse and

Item	Q_p (m^3/s)	T_p (h)	B_t (m)	B (m)	H_s (m)
Model by Zhong et al.[41]	6299.34	13.80	179.00	106.64	/
	−3.16%	−8.61%	Within	Within	/
Model by Chang et al.[13]	6737	/	247	101	45
	+3.57%	/	+9.78%	Within	+28.6%
Model proposed in this paper	6698	14.17	149.24	103.90	32.2
	+2.97%	−6.16%	Within	Within	−8.00%
Measured value	6505	15.1	145 ~ 225	100 ~ 145	35

Table 4. Comparison between calculated and measured outcomes of Tangjiashan landslide dam breach.

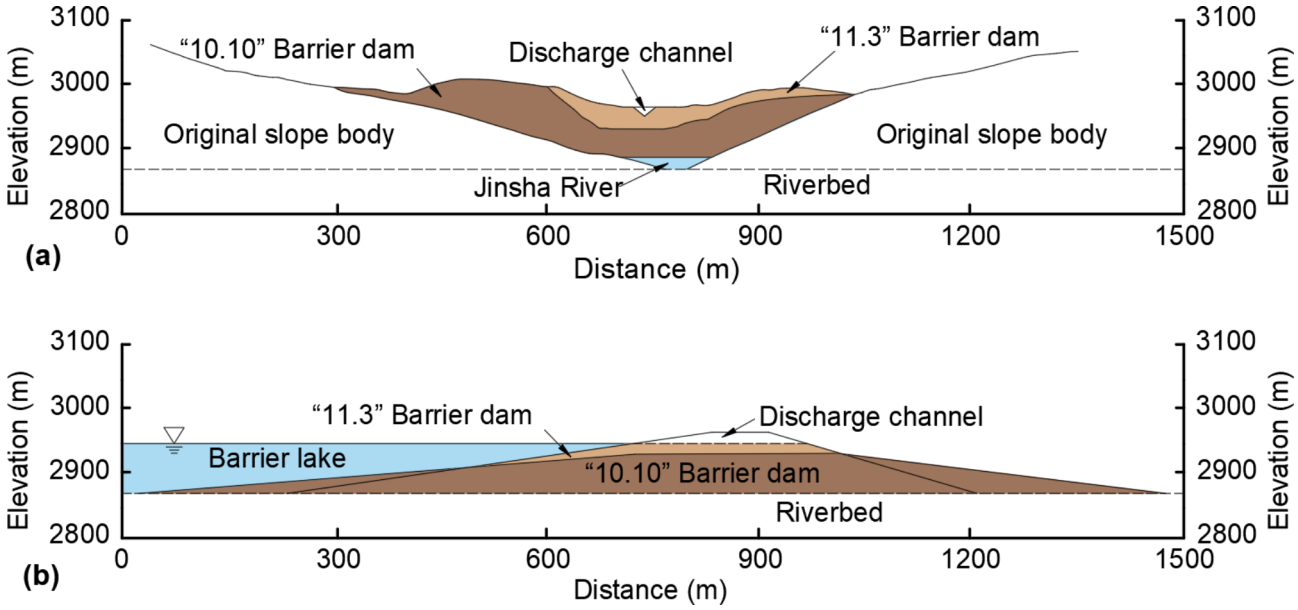

Fig. 9. The (**a**) cross-section, (**b**) longitudinal section of Baige landslide dam[53].

fine particles within the widely graded materials characteristic of landslide dams. Different particle sizes have varying thresholds for initiation and transport under water flow. When coarse and fine particles are mixed, their interactions complicate the rules governing their movement. Without incorporating micromechanical mechanisms, it becomes challenging to simplify and generalize such complex behavior for computational purposes. In previous dam breach erosion studies, highly simplified parameters such as the coefficient of erodibility (K_d) or the critical shear stress at the initiation of soil erosion (τ_c) were commonly used to approximate the erodibility of soil particles, and these were then applied in dam breach calculations[42,43]. However, the wide gradation and heterogeneity of landslide dams make it difficult to assign reasonable values to these parameters, further weakening the robustness of such models. By focusing on the interactions between particles of different sizes, the model presented in this study addresses the potential challenges posed by these oversimplified representation methods. However, the sediment transport model in this study is somewhat conservative when calculating clay erosion. This results in the overall erosion intensity calculated by the model being slightly lower than the observed data, as reflected by the smaller total discharge and the reduced final breach size. Undoubtedly, more cases are needed to comprehensively evaluate the performance of various models in different aspects, such as erosion calculation of breach soil and evolution calculation of breach water flow.

"11·3" Baige landslide dam

On October 10 and November 3, 2018, landslides occurred on the original slope of the Baige landslide dam, blocking the Jinsha River on both occasions. This study focuses on the outflow process of the "11·3" Baige landslide dam, which has comprehensive hydrological measurements and well-documented dam material properties, to further validate the model's reliability. By applying the proposed dam breach model to simulate the outflow process, the performance of the model was assessed. According to the on-site survey data, the dam height is 96 m, and the elevation at the dam crest is 2967 m. The structure of the dam is shown in Fig. 9.

The composition of the landslide dam material directly influences the erosion resistance of the dam and the breach development process. Currently, detailed information on the particle composition of the "10.11" landslide deposit is unavailable. However, since the material composition of the deposits from the "10.11" and

Particle size (mm)	The cumulative percent (%)	$P(\Delta'_l)$	$\overline{\Delta}l_l$
0.002	1.18	1.18	0.49998
0.005	2.35	1.18	0.49996
0.01	3.53	1.18	0.49991
0.02	5.88	2.35	0.49982
0.05	7.06	1.18	0.49958
0.075	8.24	1.18	0.49926
0.25	14.12	5.88	0.49806
0.5	18.24	4.12	0.49549
1	24.71	6.47	0.49090
2	30.00	5.29	0.48140
5	49.41	19.41	0.45396
10	66.47	17.06	0.60767
20	82.35	15.88	0.77033
40	95.29	12.94	0.85167
155	100.00	4.71	0.90797

Table 5. The particle composition of the "11.3" Baige landslide dam.

Parameters	Values	Parameters	Values
Dam height (m)	96	γ_w (kN/m^3)	9.8
Crest width (m)	270	γ_s (kN/m^3)	18.17
Dam length (m)	600	c (kPa)	3
U/S slope (V/H)	0.37	φ (°)	32.8
D/S slope (V/H)	0.18	n	37.5%
Reservoir storage (m^3)	7.57×10^8	C_L	0.1
Initial reservoir lever (m)	85.53	C_D	0.4
Initial downstream water lever (m)	0[a]	A_D	π/4
Initial breach depth (m)	13.48	D_L	π/4
Initial breach bottom width (m)	3	θ (°)	13[a]

Table 6. Conditions of "11.3" Baige landslide dam. [a]Assumed values.

"11.3" landslides is similar[44], this study refers to the particle gradation curve of the "11.3" landslide dam[45] and calculates the relevant parameters for the landslide dam particles, as shown in Table 5.

According to Table 5, the average particle diameter of the "11.3" Baige landslide dam is 0.488 mm. The average particle diameter D_l for each particle group is calculated as the average of the boundary particle diameters of adjacent groups. The content and the average relative exposure for each particle group are also listed in Table 5. In order to reduce the risk posed by the Baige landslide-dammed lake, a diversion channel was excavated with a top width of 42 m, a bottom width of 3 m, and a depth of 15 m, with an elevation of 2,852.52 m. The slope ratio of the channel is 1:1.3. The material properties at the breach reference a soil cohesion coefficient of 3 kPa, a soil density of 1,591 kg/m3, and a median particle size of 0.005 m. The initial water level is 2,952.56 m[46]. The model input parameters for the "11·3" Baige landslide dam are detailed in Table 6.

The outflow process of the "11.3" Baige landslide dam was simulated using the numerical calculation method proposed in this study. An iterative time step of 1 s was set, and both the breach outflow process and the breach expansion process were calculated. The results are shown in Fig. 10.

By comparing the model's calculated results with the measured data, it can be observed that the model proposed in this paper generally reflects the flow evolution characteristics and geomorphological development during the outflow process of the "11.3" Baige landslide dam. Regarding the breach outflow process, the calculated outflow develops slightly faster than the measured data at the beginning of the outflow, but the predicted peak flow and its timing align well with the observed values. For the breach development process, there is no measured data on the breach expansion during the event; only the dimensions of the residual breach after the outflow ended are available. The calculated bottom width of the residual breach matches the measured data, while the top width is slightly smaller than the observed values. Nevertheless, overall, the calculated and measured results are still in good agreement. In the calculated results, key characteristic parameters of the outflow process were extracted and compared with the measured data. The comparison results are shown in Table 7.

By analyzing the errors of the characteristic parameters during the outflow process, it can be observed that the peak breach flow and the residual breach bottom width calculated by the model are in good agreement with the measured results. The peak flow time is slightly earlier than the measured data, with an error of −4.7%. The

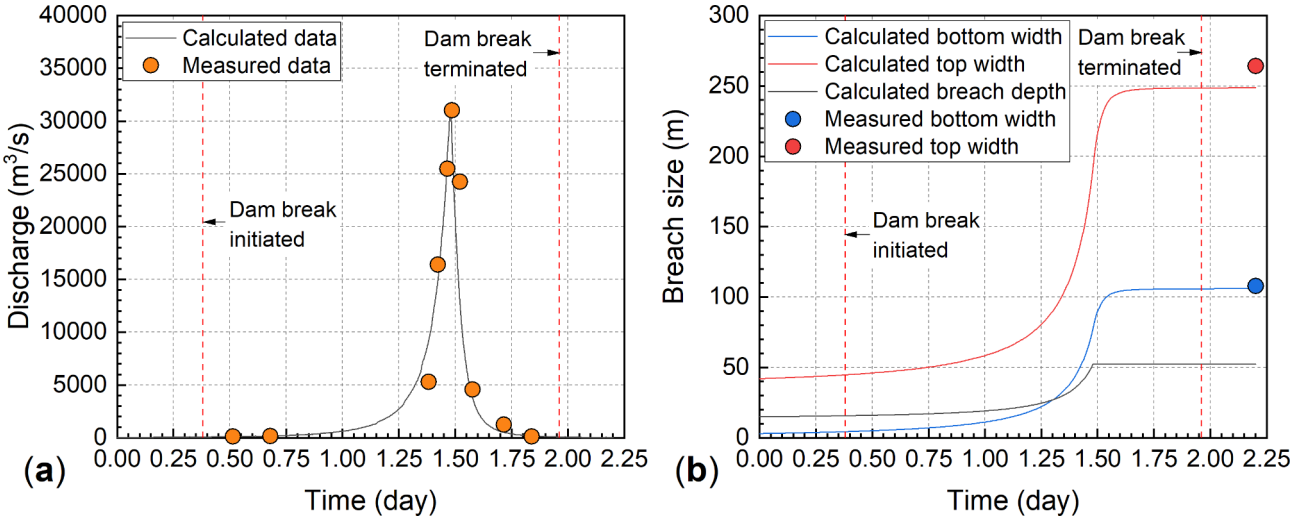

Fig. 10. Discharge process of the "11.3" Baige landslide dam: (**a**) Breach flow process; (**b**) Breach expansion process.

Item	Q_p (m^3/s)	T_p (h)	B_t (m)	B (m)
Measured value	31000	37.25	264.1	107.8
Calculated value	31678.5	35.5	248.7	105.9
Relative error	+2.2%	−4.7%	−5.8%	−1.8%

Table 7. Comparison between calculated and measured outcomes of "11.3" Baige landslide dam breach.

calculated residual breach top width is slightly smaller than the measured value. However, overall, the model accurately reflects the real outflow and dam breach process.

Yigong landslide dam

In this section, the Yigong landslide dam breach process is selected for further evaluation of the model's accuracy. The Yigong landslide dam was formed by a large-scale landslide that occurred in the Zhamunong Gully of the Yigong Zangbo River in Bomi County, Nyingchi Prefecture, Tibet, China, in 2000, which blocked the Yigong Zangbo River[47]. The landslide dam had an extremely irregular shape with an uneven surface. The dam's bottom width ranged from 2200 to 2500 m, its length along the axis was approximately 1000 m, and the dam's surface area was about 215 km^2. The dam crest was wide, with the saddle area in the flow direction exceeding 200 m in width. The dam rose 5511 m above the lake water level and approximately 90 m above the downstream slope toe. The upstream and downstream slopes were gentle, with average gradients of 5 and 8°, respectively. The geology and morphology of the landslide have been documented in various publications[48–50]. Wang et al.[16] conducted a field reconnaissance in 2014 and brought some debris material from the dam back to the laboratory. Table 8 presents the grain size distribution of the nine tested specimens.

The average particle size of the Yigong landslide dam is 8 mm. The average particle diameter D_l for each particle group is calculated as the average of the boundary particle diameters of adjacent groups. The probability density for each particle group can be calculated, allowing the exposure of each group to be determined, leading to a comprehensive exposure value of 0.625167 for the landslide dam material. The calculation results for each particle group are shown in Table 8. As mentioned earlier, the shape of the Yigong landslide dam is highly irregular, making it particularly challenging to select the parameters for breach calculations, especially the geometric parameters. Based on field investigation, the dam height ranges from 60 to 100 m, with the lowest point being 80 m high. The length along the river is between 2200 and 2500 m. When overtopping occurred, the width of the breach bottom was 5 m. Other parameters were selected based on the inversion results from Wang[16], with specific values listed in Table 9.

Based on the parameters listed in Table 9, the breach process of the Yigong landslide dam was simulated using the dam breach model proposed in this study. Since the Yigong landslide dam occurred in a remote area and took place a long time ago, detailed records of the breach process are incomplete. Therefore, the focus of the calculation results is on the documented aspects of the breach, particularly the outflow process and the lateral widening of the breach, as shown in Fig. 11.

Regarding the breach flow process, the calculated breach flow initially shows a slower rate of increase compared to the measured results. However, once the outflow begins, the breach flow increases rapidly and quickly reaches a peak. The peak flow obtained from the calculations is slightly higher than the measured peak flow, and the peak occurs slightly earlier than in the measurements. During the flow recession phase, the

Particle size (mm)	The cumulative percent (%)	$P(\Delta'_l)$	$\overline{\Delta}l_l$
0.075	2.84616	2.85	0.49946
0.25	16.4215	13.58	0.49882
1	27.3559	10.93	0.49542
2	31.0042	3.65	0.48884
4	38.9506	7.95	0.47709
5	40.2771	1.33	0.46470
10	54.6698	14.39	0.43779
20	65.095	10.43	0.66633
40	78.0004	12.91	0.79967
60	87.2636	9.26	0.85300
100	100	12.74	0.88300

Table 8. The particle composition of the Yigong landslide dam.

Parameters	Values	Parameters	Values
Dam height (m)	100	γ_w (kN/m^3)	9.8
Crest width (m)	200	γ_s (kN/m^3)	18.08
Dam length (m)	2500	c (kPa)	13
U/S slope (V/H)	0.0875	φ (°)	37
D/S slope (V/H)	0.141	n	37.5%[a]
Reservoir storage (m^3)	2.38×10^9	C_L	0.1
Initial reservoir lever (m)	80.65	C_D	0.4
Initial downstream water lever (m)	0[a]	A_D	π/4
Initial breach depth (m)	20[a]	D_L	π/4
Initial breach bottom width (m)	5	θ (°)	13[a]

Table 9. Conditions of Yigong landslide dam. [a]Assumed values.

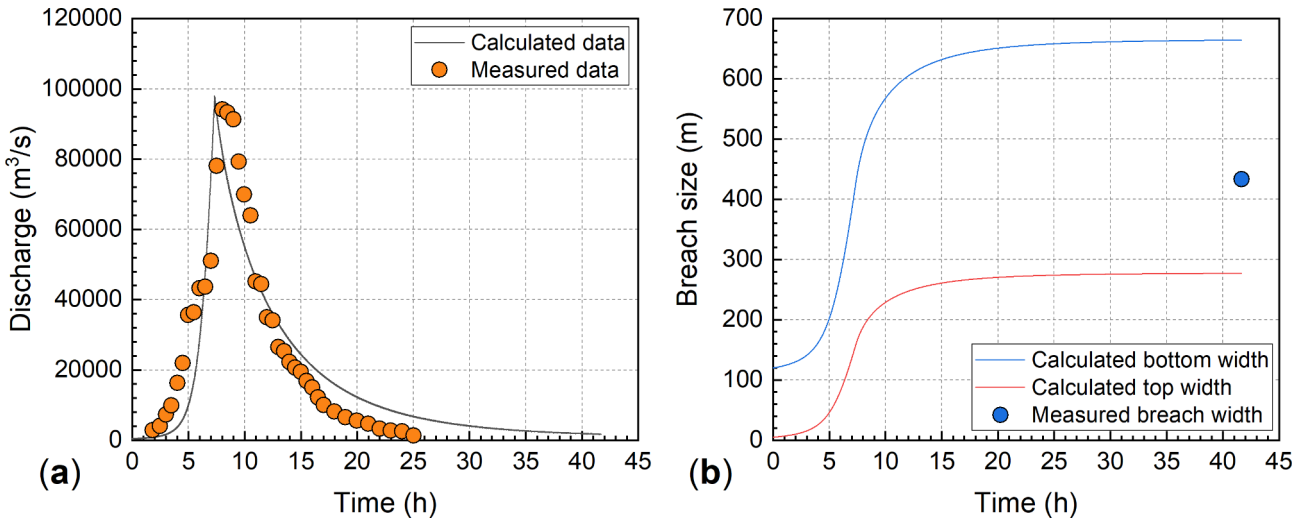

Fig. 11. Discharge process of the Yigong landslide dam: (**a**) Breach flow process; (**b**) Breach expansion process.

calculated flow decreases more slowly. Nevertheless, the overall flow process reflects the measured results. As for the lateral widening of the breach, only the final width of the breach after the dam failure was recorded, without distinguishing between the top and bottom widths. The calculated residual breach widths for the top and bottom are on either side of the measured result.

Key parameters during the dam breach process were selected and compared with the measured data, as shown in Table 10. From the table, the calculated peak flow is 4.2% higher than the measured result, and the peak time is 8.3% earlier, indicating that the calculated results are more conservative and safer. As for the residual

Item	Q_p (m^3/s)	T_p (h)	B_t (m)	B (m)
Measured value	94013	8.00	433	
Calculated value	97953.86	7.33	664	277
Relative error	+4.2%	−8.3%	/	/

Table 10. Comparison between calculated and measured outcomes of Yigong landslide dam breach.

	Gradation 1 (Prototype)		Gradation 2		Gradation 3	
Particle size (mm)	$P(\Delta'_l)$ (%)	$\overline{\Delta}_l$	$P(\Delta'_l)$ (%)	$\overline{\Delta}_l$	$P(\Delta'_l)$ (%)	$\overline{\Delta}_l$
0.005	4.66867	0.49999	4.66867	0.49998	4.66867	0.49998
0.075	8.10240	0.49990	8.44667	0.49988	9.72104	0.49981
0.25	4.39761	0.49959	4.58446	0.49951	5.27613	0.49924
0.5	1.47590	0.49906	1.53861	0.49886	1.77075	0.49825
2	5.48193	0.49684	5.71486	0.49618	6.57707	0.49410
5	9.33735	0.49103	9.73409	0.48912	11.20269	0.48305
10	6.89758	0.48031	7.19066	0.47600	8.27553	0.46198
20	8.52412	0.45875	8.88631	0.44919	10.22700	0.41664
40	7.13854	0.54783	7.44186	0.38488	8.56462	0.29352
60	3.70480	0.70190	3.86222	0.74160	4.44492	0.80850
100	24.39762	0.78856	25.43428	0.81338	29.27159	0.85519
200	11.98794	0.85597	12.49731	0.86920	/	/
250	3.88554	0.88164	/	/	/	/

Table 11. Relative exposure of different gradation widths. The average particle size values $\overline{D}$ are: 23.11 mm for Gradation 1, 19.14 mm for Gradation 2, and 12.45 mm for Gradation 3.

breach width after the dam failure, no error analysis could be performed between the calculated and measured results. However, the average of the calculated top and bottom breach widths is close to the measured result, showing reasonable consistency.

Influence of particles gradation width

From the comparison in the previous section, it's evident that the material parameters of the dam significantly impact the calculation results of dam failure. Considering the wide-graded soil erosion can further enhance the accuracy of simulation results. In fact, the wide gradation of materials has a direct impact on the erodibility of soil, as it affects the average particle size $\overline{D}$ directly in the model. For landslide dams containing clay, the wider the particle size distribution, the larger the average particle size, making it more difficult for particles to start moving under the erosion of overtopping flow, indicating weaker erodibility. Additionally, the wider the particle size distribution range, the more significant the shielding and exposure effects between particles of different sizes, leading to different relative exposure Δ' values of particles in the model.

According to Eq. (6), the average particle size and exposure are related and both are affected by the grading width of the dam particles. To comprehensively study the effects of average particle size and exposure on the dam failure process, this section conducts dam failure calculations on dams composed of particles with different gradation widths and investigates the influence of gradation widths on the dam failure process.

Based on the particle size distribution of the Tangjiashan landslide dam materials (Gradation 1), with maximum particle sizes controlled at 200 and 100 mm respectively, the equal-proportion replacement method was employed. To maintain the soil properties unchanged, the content of clay particles (i.e., particles with a diameter less than 0.005 mm) remains constant. Other finer particle groups were used to proportionally replace the particles exceeding the maximum size controlled to obtain Gradation 2 and 3. $\Delta\prime_m$ retains a value of 0.134. The relative exposure of each particle group was then calculated to obtain the comprehensive relative exposure for each gradation. The results are shown in Table 11.

Based on the data presented in Table 11, the weighted average method can be employed to calculate the comprehensive relative exposure of the three gradations, yielding values of 0.633, 0.619, and 0.586, respectively. It's apparent that the comprehensive relative exposure decreases gradually with a reduction in gradation width. Except for parameters $\overline{D}$ and $\overline{\Delta}\prime$, the selection of other parameters is detailed in Table 3. The models proposed were applied to calculate the dam failure processes for Gradations 1, 2, and 3, respectively, and the calculation results are presented in Fig. 12.

From Fig. 12, it is evident that as the gradation width decreases, the average particle size of the dam gradually reduces, leading to a decrease in particle exposure. Consequently, there is a sharp increase in the peak discharge of the breach, accompanied by a notable advancement in the peak time. The discharge acceleration during the breach rising stage is pronounced, and the water level recession rate accelerates after the peak discharge. Moreover,

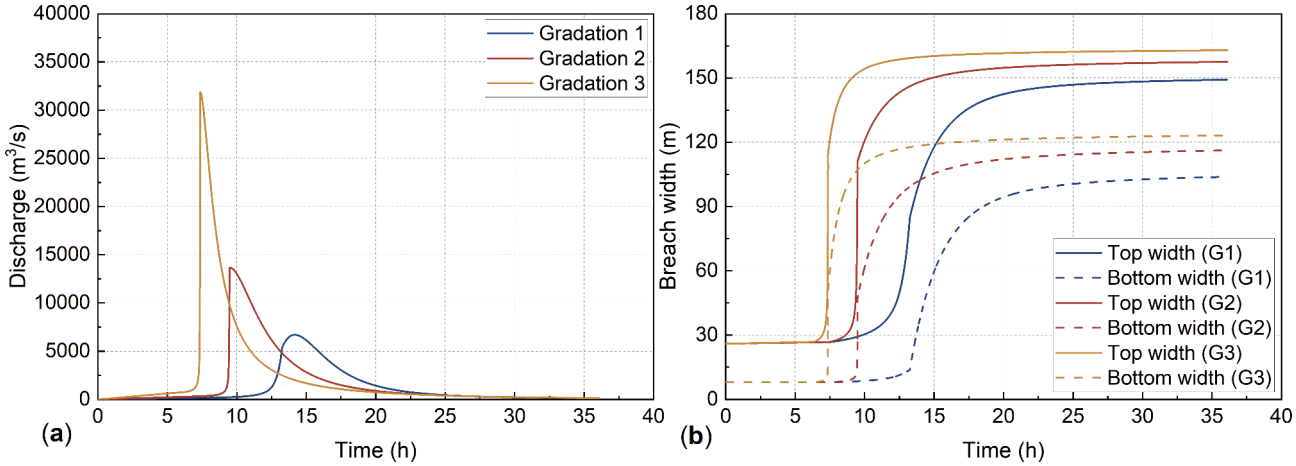

Fig. 12. The failure process of Tangjiashan landslide dam under different gradation widths: (**a**) Discharge of breach; (**b**) Development of breach.

Gradations	d_{100} (mm)	$\overline{\Delta}/$	Q_p (m³/s)	T_p (h)	B_t (m)	B (m)
1 (Prototype)	250	0.633	6698.00	14.13	149.24	103.90
	/	/	/	/	/	/
2	200	0.619	13679.23	9.48	157.57	116.26
	−20%	−2.2%	+104.23%	−32.90%	+5.60%	+11.90%
3	100	0.586	31883.20	7.36	162.93	123.22
	−60%	−7.4%	+376.01%	−47.91%	+9.17%	+18.60%

Table 12. Comparison of calculated outcomes under different gradation widths. d_{100} is the maximum particle size of the dam material.

as the gradation width decreases, the start time of the expansion of the breach top and bottom continually advances, and the expansion rate increases. In other words, the decrease in gradation width significantly enhances the erosion intensity of the breach. Finally, the width of the breach after dam failure increases continuously as the gradation width decreases. Key outcomes for dam failure under the three gradations are listed in Table 12.

According to Table 12, the gradation width of the dam material has a significant impact on the dam failure development process, especially on the discharge process of the breach. The reduction in the maximum particle size of the dam material and its relative exposure to some extent can lead to a substantial increase in the peak discharge, nearly fivefold, and cause a similar degree of advance in the peak time. In comparison to the flow through the breach, the variation in gradation width has a relatively minor effect on the width of the breach, indicating a low sensitivity of residual breach size to the gradation width of the dam material.

Discussion

Developing a widely applicable mathematical model often first requires addressing the model's inherent complexity and solvability. To balance complexity and solvability, this study adopts a series of assumptions. Specifically, for the sediment transport model, the calculation of relative exposure considers both the lateral exposure angle (α) and the longitudinal exposure angle (β). However, since landslide dams consist of a mixture of coarse and fine particles, it is difficult to distinguish between and assign values to these exposure angles in practice. To simplify the computation of relative exposure and facilitate its application, this study assumes that the particle distribution follows a statistically self-similar pattern, with equal lateral and longitudinal exposure angles. Based on the validation of the incipient motion velocity and sediment transport formulas, this assumption has minimal impact on the overall accuracy of the results.

Moreover, the validation of the incipient motion velocity formula shows that the proposed formula accurately predicts the initiation of sand particles but underestimates the initiation velocity for clay particles. According to our analysis, the gap size between particles still requires further refinement, as even clay particles exhibit a wide range of particle sizes that span two orders of magnitude. Nonetheless, the current incipient motion formula is still able to reflect real-world conditions when calculating the unit sediment transport rate. Therefore, based on the current validation results of the sediment transport formula, the model can maintain a high level of accuracy when simulating overtopping-induced dam failure in widely graded landslide dams. However, its applicability to homogeneous dams with a high clay content still requires validation through additional real-world case studies, and care should be taken when selecting this model for such cases.

For the outflow and breach development module, several assumptions underpin the proposed model. Specifically, the breach is assumed to have a regular trapezoidal shape. Additionally, the scouring of the breach sidewalls and base by overtopping flow does not account for the effects of flow depth, and the breach is treated as a full-cross-section flow. As such, further discussion on the calculation of breach top width expansion is needed in future studies. Regarding breach collapse, it is assumed that the sliding surface is planar and passes through the base of the breach sidewalls. Whether this assumption holds for homogeneous dams with high clay content remains to be further investigated. For such dams, the effects of overtopping flow on sidewall saturation and its impact on the shear strength of clay must be considered, making the collapse mechanism of the breach sidewalls more complex.

Conclusion remarks

In this study, we propose a new model for predicting the process of overtopping failure in landslide dams. In this model, particular emphasis is placed on the scouring of wide-graded materials. By introducing the relative exposure under three-dimensional conditions, we calculate the critical flow velocity of wide-graded soil to overcome the limitations of erosion formulas used in current dam breach models, which fail to account for the interaction between particles in wide-graded soil. This can further enhance the accuracy of dam failure process calculations, especially for landslide dams containing wide-graded soil.

The performance of the model was evaluated using the discharge process of Tangjiashan landslide dam. The results show that the calculated breach discharge process, breach development process, reservoir water level development process, and discharge volume are close to the measured results, indicating that the model can simulate the overtopping failure process of landslide dams to a certain extent. Furthermore, the calculated results of this study model were compared with two other existing models, showing that the key dam failure parameters calculated in this study can be controlled within a smaller error range, which is attributed to the comprehensive consideration of scouring of wide-graded soil in our model. Additionally, two additional real-world cases, the "11.3" Baige landslide dam and the Yigong landslide dam, were selected for breach calculations, and the dam failure results still demonstrated reasonable consistency. Additionally, the impact of the gradation width of the dam material on the dam failure process was studied using the proposed model. The results indicate that the gradation width of the dam material has a significant effect on the flow of the breach, indicating a high sensitivity of breach flow to gradation width. However, the residual breach width is less affected by gradation width, showing weaker sensitivity.

While the model proposed in this research performs well in simulating the discharge process of Tangjiashan landslide dam, it is undeniable that further validation of the proposed model is needed through more real-world cases and comprehensive comparisons with existing dam breach models. Moreover, the accurate calculation of sediment initiation and transport for landslide dams with high clay content requires further investigation in future studies. In addition, there is currently no unified method for quantitatively representing the gradation width of soil and rock materials. In this study, when investigating the impact of gradation width on the dam failure process, we utilized the maximum particle size (while keeping the minimum particle size and its content unchanged) and the comprehensive relative exposure of particles. However, it can be observed that these two factors exhibit different sensitivities in representing the gradation width of soil and rock materials, which poses challenges for sensitivity analysis of key dam failure outcomes. Developing a unified method to characterize gradation width will be an interesting topic for future research.

Data availability

The input parameters and output results of the breach model used for real-world dam break calculation in this paper are available from the digital data repository in Zhao[50].

Appendix A

Calculation parameter values for (Fig. 5a).

q_b (m^2/s)	θ	H (m)	B (m)	d_{90} (m)	d_{90}/d_{30}	γ_s (kN/m^3)	γ_w (kN/m^3)
0.0242	0.100	0.031	0.2	0.0052	1.44	26.166	9.8
0.0246	0.200	0.034	0.2	0.0052	1.44	26.166	9.8
0.0452	0.050	0.041	0.2	0.0052	1.44	26.166	9.8
0.0469	0.100	0.040	0.2	0.0052	1.44	26.166	9.8
0.0487	0.200	0.054	0.2	0.0052	1.44	26.166	9.8
0.0688	0.100	0.049	0.2	0.0052	1.44	26.166	9.8
0.0835	0.030	0.068	0.2	0.0052	1.44	26.166	9.8
0.0844	0.050	0.055	0.2	0.0052	1.44	26.166	9.8
0.0873	0.070	0.055	0.2	0.0052	1.44	26.166	9.8
0.0895	0.100	0.054	0.2	0.0052	1.44	26.166	9.8
0.0931	0.150	0.061	0.2	0.0052	1.44	26.166	9.8
0.0948	0.200	0.064	0.2	0.0052	1.44	26.166	9.8
0.1105	0.100	0.062	0.2	0.0052	1.44	26.166	9.8
0.1293	0.100	0.065	0.2	0.0052	1.44	26.166	9.8

Appendix B

Calculation parameter values for (Fig. 5b).

q_b (m²/s)	θ	H (m)	B (m)	d_{90} (m)	d_{90}/d_{30}	γ_s (kN/m³)	γ_w (kN/m³)
0.0241	0.105	0.029	0.2	0.0121	1.34	26.264	9.8
0.0237	0.150	0.019	0.2	0.0121	1.34	26.264	9.8
0.0246	0.200	0.037	0.2	0.0121	1.34	26.264	9.8
0.0466	0.070	0.045	0.2	0.0121	1.34	26.264	9.8
0.0476	0.100	0.048	0.2	0.0121	1.34	26.264	9.8
0.0481	0.150	0.046	0.2	0.0121	1.34	26.264	9.8
0.0489	0.200	0.059	0.2	0.0121	1.34	26.264	9.8
0.0635	0.034	0.051	0.2	0.0121	1.34	26.264	9.8
0.0678	0.070	0.054	0.2	0.0121	1.34	26.264	9.8
0.0703	0.100	0.059	0.2	0.0121	1.34	26.264	9.8
0.0712	0.150	0.057	0.2	0.0121	1.34	26.264	9.8
0.0725	0.200	0.066	0.2	0.0121	1.34	26.264	9.8
0.0848	0.036	0.066	0.2	0.0121	1.34	26.264	9.8
0.0874	0.050	0.066	0.2	0.0121	1.34	26.264	9.8
0.0869	0.074	0.052	0.2	0.0121	1.34	26.264	9.8
0.0895	0.100	0.054	0.2	0.0121	1.34	26.264	9.8
0.0946	0.150	0.072	0.2	0.0121	1.34	26.264	9.8
0.0956	0.200	0.073	0.2	0.0121	1.34	26.264	9.8
0.1100	0.070	0.072	0.2	0.0121	1.34	26.264	9.8
0.1131	0.100	0.072	0.2	0.0121	1.34	26.264	9.8
0.1162	0.150	0.074	0.2	0.0121	1.34	26.264	9.8
0.1179	0.200	0.075	0.2	0.0121	1.34	26.264	9.8
0.1294	0.070	0.078	0.2	0.0121	1.34	26.264	9.8
0.1329	0.100	0.075	0.2	0.0121	1.34	26.264	9.8
0.1362	0.150	0.073	0.2	0.0121	1.34	26.264	9.8
0.1398	0.200	0.079	0.2	0.0121	1.34	26.264	9.8

Appendix C

Calculation parameter values for (Fig. 5c).

q_b (m²/s)	θ	H (m)	B (m)	d_{90} (m)	d_{90}/d_{30}	γ_s (kN/m³)	γ_w (kN/m³)
0.0240	0.100	0.028	0.2	0.0046	4.60	26.264	9.8
0.0458	0.100	0.032	0.2	0.0046	4.60	26.264	9.8
0.0475	0.200	0.033	0.2	0.0046	4.60	26.264	9.8
0.0683	0.100	0.046	0.2	0.0046	4.60	26.264	9.8
0.0832	0.050	0.052	0.2	0.0046	4.60	26.264	9.8
0.0852	0.070	0.049	0.2	0.0046	4.60	26.264	9.8
0.0881	0.100	0.048	0.2	0.0046	4.60	26.264	9.8
0.0912	0.150	0.050	0.2	0.0046	4.60	26.264	9.8
0.0938	0.200	0.056	0.2	0.0046	4.60	26.264	9.8
0.1067	0.100	0.051	0.2	0.0046	4.60	26.264	9.8
0.1271	0.100	0.059	0.2	0.0046	4.60	26.264	9.8

Appendix D

Calculation parameter values for (Fig. 5d).

q_b (m²/s)	θ	H (m)	B (m)	d_{90} (m)	d_{90}/d_{30}	γ_s (kN/m³)	γ_w (kN/m³)
0.0240	0.070	0.034	0.2	0.0110	8.46	26.166	9.8
0.0241	0.100	0.029	0.2	0.0110	8.46	26.166	9.8
0.0243	0.150	0.029	0.2	0.0110	8.46	26.166	9.8
0.0246	0.200	0.034	0.2	0.0110	8.46	26.166	9.8
0.0440	0.030	0.044	0.2	0.0110	8.46	26.166	9.8
0.0468	0.070	0.047	0.2	0.0110	8.46	26.166	9.8
0.0476	0.100	0.048	0.2	0.0110	8.46	26.166	9.8

q_b (m²/s)	θ	H (m)	B (m)	d_{90} (m)	d_{90}/d_{30}	γ_s (kN/m³)	γ_w (kN/m³)
0.0482	0.150	0.048	0.2	0.0110	8.46	26.166	9.8
0.0486	0.200	0.049	0.2	0.0110	8.46	26.166	9.8
0.0638	0.030	0.055	0.2	0.0110	8.46	26.166	9.8
0.0680	0.070	0.053	0.2	0.0110	8.46	26.166	9.8
0.0683	0.100	0.046	0.2	0.0110	8.46	26.166	9.8
0.0700	0.150	0.047	0.2	0.0110	8.46	26.166	9.8
0.0720	0.200	0.058	0.2	0.0110	8.46	26.166	9.8
0.0878	0.070	0.057	0.2	0.0110	8.46	26.166	9.8
0.0881	0.100	0.048	0.2	0.0110	8.46	26.166	9.8
0.0939	0.150	0.066	0.2	0.0110	8.46	26.166	9.8
0.0945	0.200	0.061	0.2	0.0110	8.46	26.166	9.8
0.1060	0.070	0.059	0.2	0.0110	8.46	26.166	9.8
0.1105	0.100	0.062	0.2	0.0110	8.46	26.166	9.8
0.1143	0.150	0.064	0.2	0.0110	8.46	26.166	9.8
0.1179	0.200	0.075	0.2	0.0110	8.46	26.166	9.8
0.1230	0.070	0.061	0.2	0.0110	8.46	26.166	9.8
0.1329	0.100	0.075	0.2	0.0110	8.46	26.166	9.8
0.1384	0.150	0.083	0.2	0.0110	8.46	26.166	9.8
0.1406	0.200	0.084	0.2	0.0110	8.46	26.166	9.8

Received: 23 August 2024; Accepted: 4 November 2024
Published online: 08 November 2024

References

1. Ren, Q., Chen, S. S., Zong, Q. M. & Cao, W. Formation mechanism and breaching failure risk of barrier dams. *Adv. Sci. Technol. Water Resour.* **31** (5), 30–34 (2011).
2. Yan, Z. W., Wei, Y. Q. & Cai, H. Formation mechanism and stability analysis of barrier dam. *Ch. J. Geol. Hazard Control* **20** (04), 55–59 (2009).
3. Schuster, R. L. & Costa, J. E. A perspective on landslide dams. In *Paper Presented at the Landslide Dams: Processes, Risk, and Mitigation* (eds Schuster, R. L. & Costa, J. E.) (Seattle, 1986).
4. Chen, H., Ruan, H., Chen, J., Li, X. & Yu, Y. Review of investigations on hazard chains triggered by river-blocking debris flows and dam-break floods. *Front. Earth Sci.* **10**, 830044 (2022).
5. Chen, S. S., Chen, Z. Y. & Zhong, Q. M. Progresses of studies on failure mechanism and numerical dam failure model of earth-rockfill dam and landslide dam. *Water Resour. Hydropow. Eng.* **50** (08), 27–36 (2019).
6. Zhong, Q. M., Chen, X. K., Mei, S. Y., Shan, Y. B. & Du, Z. H. A state of the art review on the failure risk and process of the landslide-induced dammed lake. *Adv. Water Sci.* **33** (4), 659–670 (2022).
7. Evans, S. G. The maximum discharge of outburst floods caused by the breaching of man-made and natural dams. *Canadian Geotech. J.* **23** (3), 385–387. https://doi.org/10.1139/t86-053 (1986).
8. Froehlich, D. C. Peak outflow from breached embankment dam. *J. Water Resour. Plan. Manag.* **121** (1), 90–97 (1995).
9. MacDonald, T. C. & Monopolis, J. L. Breaching charateristics of dam failures. *J. Hydraulic Eng.* **110** (5), 567–586. https://doi.org/10.1061/(ASCE)0733-9429(1984)110:5(567) (1984).
10. Mei, S., Chen, S., Zhong, Q. & Yan, Z. Parametric model for breaching analysis of earth-rock dam. *Adv. Eng. Sci.* **50** (02), 60–66 (2018).
11. Ruan, H., Chen, H., Wang, T., Chen, J. & Li, H. Modeling flood peak discharge caused by overtopping failure of a landslide dam. *Water* **13** (7), 921 (2021).
12. Walder, J. S. & O'Connor, J. E. Methods for predicting peak discharge of floods caused by failure of natural and constructed earthen dams. *Water Resour. Res.* **33** (10), 2337–2348 (1997).
13. Chang, D. & Zhang, L. Simulation of the erosion process of landslide dams due to overtopping considering variations in soil erodibility along depth. *Nat. Hazards Earth Syst. Sci.* **10** (4), 933–946 (2010).
14. Chen, S. S., Zhao, T. L. & Zhong, Q. M. Dam-break numerical model for a barrier dam and its application. *Hydro Sci. Eng.* **3**, 1–8 (2015).
15. Chen, Z. et al. Back analysis of the draining process of the tangjiashan barrier lake. *J. Hydraulic Eng.* https://doi.org/10.1061/(ASCE)HY.1943-7900.0000965 (2015).
16. Wang, L. et al. Modeling lateral enlargement in dam breaches using slope stability analysis based on circular slip mode. *Eng. Geol.* **209**, 70–81 (2016).
17. Wu, W. Simplified physically based model of earthen embankment breaching. *J. Hydraulic Eng.* **139**, 837–851 (2013).
18. Zhong, Q., Wu, W., Chen, S. & Wang, M. Comparison of simplified physically based dam breach models. *Nat. Hazards* **84** (2), 1385–1418. https://doi.org/10.1007/s11069-016-2492-9 (2016).
19. Faeh, R. Numerical modeling of breach erosion of river embankments. *J. Hydraulic Eng.* **133** (9), 1000–1009. https://doi.org/10.1061/(ASCE)0733-9429(2007)133:9(1000) (2007).
20. Swartenbroekx, C., Soares-Frazão, S., Staquet, R. & Zech, Y. Two-dimensional operator for bank failures induced by water-level rise in dam-break flows. *J. Hydraulic Res.* **48** (3), 302–314. https://doi.org/10.1080/00221686.2010.481856 (2010).
21. Wang, Z. & Bowles, D. S. Three-dimensional non-cohesive earthen dam breach model. Part 1: Theory and methodology. *Adv. Water Resour.* **29** (10), 1528–1545 (2006).
22. Wu, W. & Wang, S. S. One-dimensional modeling of dam-break flow over movable beds. *J. Hydraulic Eng.* **133** (1), 48–58. https://doi.org/10.1061/(ASCE)0733-9429(2007)133:1(48) (2007).
23. Wu, W., Marsooli, R. & He, Z. Depth-averaged two-dimensional model of unsteady flow and sediment transport due to noncohesive embankment break/breaching. *J. Hydraulic Eng.* **138** (6), 503–516. https://doi.org/10.1061/(ASCE)HY.1943-7900.0000546 (2012).

24. Zhao, T., Ma, T., Fu, C. & Zhang, C. Experimental study on wide-graded soil transport in unsteady flow. *Processes* **11** (7), 1965. https://doi.org/10.3390/pr11071965 (2023).
25. Khosravi, K. et al. Uniform and graded bed-load sediment transport in a degrading channel with non-equilibrium conditions. *Int. J. Sed. Res.* **35** (2), 115–124 (2020).
26. Zhang, L. et al. A comparison study between 2D and 3D slope stability analyses considering spatial soil variability. *J. Zhejiang Univ. Sci A* **23** (3), 208–224 (2022).
27. Han, Q. W. & He, M. M. *The law and velocity of sediment initiation* (Science Press, 1999).
28. Li, L. & Zhang, G. A Unified formula of sediment incipient velocity on slopes. *J. Yangtze River Sci. Res. Inst.* **35** (04), 13–17 (2018).
29. Hu, X. et al. Experimental and numerical study on the breaching mechanisms of landslide dams with non-uniform structures. *Eng. Geol.* **330**, 107414 (2024).
30. Singh, V. P. Dam breach modeling technology. In *Water Science and Technology Library* (ed. Singh, V. P.) (Springer, 1996).
31. Singh, K. P. & Snorrason, A. Sensitivity of outflow peaks and flood stages to the selection of dam breach parameters and simulation models. *J. Hydrol.* **68** (1–4), 295–310 (1984).
32. Dou, G. On the incipient motion velocity of sediment. *J. Hydraulic Eng.* **04**, 46–62 (1960).
33. Han, Q. Characteristics of incipient sediment motion and incipient velocity. *J. Sediment Res.* **02**, 13–28 (1982).
34. Smart, G. M. Sediment transport formula for steep channels. *J. Hydraulic Res.* **110** (03), 267–276 (1984).
35. Cui, P. et al. Landslide-dammed lake at Tangjiashan, Sichuan province, China (triggered by the Wenchuan Earthquake, May 12, 2008): risk assessment, mitigation strategy, and lessons learned. *Environ. Earth Sci.* **65** (4), 1055–1065 (2012).
36. Ding, Z. X. & Wang, Y. C. Analysis of submergence and disaster assessment on landslide·dammed lake reservoir area based on remote sensing and GIS. *Water Resour. Hydropower Eng.* **10**, 116–120 (2008).
37. Liu, N. et al. Draining the Tangjiashan barrier lake. *J. Hydraulic Eng.* **136** (11), 914–923 (2010).
38. Hu, X. W. et al. Analysis of blocking river mechanism of tangjiashan landslide and dam-breaking mode of its barrier dam. *Chin. J. Rock Mech. Eng.* **28** (1), 181–189 (2009).
39. Liu, N., Zhang, J., Lin, W., Chen, W. & Chen, Z. Draining Tangjiashan Barrier Lake after Wenchuan Earthquake and the flood propagation after the dam break. *Sci. China Ser E-Tech Sci* **39** (08), 1359–1366 (2009).
40. Zhong, Q. M., Chen, S. S., Mei, S. A. & Cao, W. Numerical simulation of landslide dam breaching due to overtopping. *Landslides* **15**, 1183–1192 (2018).
41. Chang, D. S., Zhang, L. M., Xu, Y. & Huang, R. Q. Field testing of erodibility of two landslide dams triggered by the 12 May Wenchuan earthquake. *Landslides* **8** (3), 321–332 (2011).
42. Wang, B., Yang, S. & Chen, C. Landslide dam breaching and outburst floods: A numerical model and its application. *J. Hydrol.* **609**, 127733 (2022).
43. Xie, C. et al. Numerical simulation of the natural erosion and breaching process of the "10.11" Baige landslide dam on the Jinsha River. *Yangtze River* **52** (08), 22–29 (2021).
44. Cai, Y. et al. Study on structural morphology and dam-break characteristics of Baige barrier dam on Jinsha River. *Yangtze River* **50** (03), 15–22 (2019).
45. Zhang, L., Xiao, T., He, J. & Chen, C. Erosion-based analysis of breaching of Baige landslide dams on the Jinsha River, China, in 2018. *Landslides* **16** (10), 1965–1979 (2019).
46. Yin, Y. Overview of the Giant Landslide on the Yigong expressway in Bomi Tibet. *Ch. J. Geo Logical Hazard Control* **11** (2), 100 (2000).
47. Shang, Y. et al. A super-large landslide in Tibet in 2000: background, occurrence, disaster, and origin. *Geomorphology* **54** (3), 225–243 (2003).
48. Turzewski, M. D., Huntington, K. W. & LeVeque, R. J. The geomorphic impact of outburst floods: integrating observations and numerical simulations of the 2000 Yigong Flood, Eastern Himalaya. *J. Geophys. Res. Earth Surface* **124** (5), 1056–1079 (2019).
49. Wen, B., Wang, S., Wang, E. & Zhang, J. Characteristics of rapid giant landslides in China. *Landslides* **1** (4), 247–261 (2004).
50. Zhao T. Dataset for Simulation of Landslide Dam Failure Due to Overtopping Considering Wide-Graded Soil Erosion. https://figshare.unimelb.edu.au/articles/dataset/Dataset_for_Simulation_of_Landslide_Dam_Failure_Due_to_Overtopping_Considering_Wide-Graded_Soil_Erosion/27215025?file=49757223 (2024).
51. Tang, C. Sediment incipient motion laws. *J. Hydraulic Eng.* **2** (1), 1–12 (1963).
52. Zhong, Q., Chen, S. & Shan, Y. Numerical modeling of breaching process of baige dammed lake on Jinsha River. *Adv. Eng. Sci.* **52** (2), 29–37 (2020).
53. Bai, Y., Chen, Y. & Han, Q. Bed load saltation movement mechanism. *J. Tianjin Univ.* **45** (03), 196–201 (2012).

Acknowledgements

The authors gratefully acknowledge financial support from the Chongqing Water Conservancy Science and Technology Project (CQSLK-2023003, CQSLK-2022028), and the National Natural Science Foundation of China (52279095, 52109149).

Author contributions

G. Song, and T. Zhao planned the campaign; G. Song, T. Zhao, P. Zhao and C. Fu developed mathematical models; C. Fu and X. Hu analyzed the data; G. Song and T. Zhao wrote the manuscript draft; P. Zhao and C. Fu reviewed and edited the manuscript.

Declarations

Competing interests

The authors declare no competing interests.

Additional information

Correspondence and requests for materials should be addressed to G.S.

Reprints and permissions information is available at www.nature.com/reprints.